Article:
Bose, D.A. orcid.org/0000-0002-0276-6486, Donahue, G., Reinberg, D. et al. (3 more authors) (2017) RNA Binding to CBP Stimulates Histone Acetylation and Transcription. Cell, 168 (1-2). 135-149.e22. ISSN 0092-8674

https://doi.org/10.1016/j.cell.2016.12.020

RNA binds to a CBP regulatory motif to stimulate histone acetylation and transcription

[1,2]Daniel A Bose, [1,2]Greg Donahue, [3]Danny Reinberg, [4]Ramin Shiekhattar, [1,2]Roberto Bonasio, [1,2,5]Shelley L Berger

Affiliations

[1]Cell and Developmental Biology, Perelman School of Medicine, University of Pennsylvania, Philadelphia, Pennsylvania 19104, USA.

[2]Epigenetics Program, Perelman School of Medicine, University of Pennsylvania, Philadelphia, Pennsylvania 19104, USA.

[3]Department of Molecular Pharmacology and Biochemistry, New York University School of Medicine, New York, NY 10016, USA.

[4]University of Miami Miller School of Medicine, Sylvester Comprehensive Cancer Center, Department of Human Genetics, Biomedical Research Building, Room 719, 1501 NW 10th Avenue, Miami, Florida 33136, USA.

[5]Lead Contact.

Contact Information

Correspondence and requests for materials should be addressed to SLB (bergers@upenn.edu).

Summary

CBP/p300 are transcription co-activators whose binding is a signature of enhancers, *cis*-regulatory elements that control patterns of gene expression in multicellular organisms. Active enhancers produce bi-directional enhancer RNAs (eRNAs) and display CBP/p300 dependent histone acetylation. Here, we demonstrate that CBP binds directly to RNAs *in vivo* and *in vitro*. RNAs bound to CBP *in vivo* include a large number of eRNAs. Using steady-state histone acetyltransferase (HAT) assays we show that an RNA binding region in the HAT domain of CBP—a regulatory motif unique to CBP/p300—allows RNA to stimulate CBP's HAT activity. At enhancers where CBP interacts with eRNAs, stimulation manifests in RNA-dependent changes in the histone acetylation mediated by CBP, such as H3K27ac, and by corresponding changes in gene expression. By interacting directly with CBP, eRNAs contribute to the unique chromatin structure at active enhancers, which in turn is required for regulation of target genes.

Introduction

Enhancers confer spatiotemporal specificity to gene expression and orchestrate gene expression patterns in response to environmental and/or developmental stimuli (Lam et al., 2014). Enhancers account for the majority of transcription factor binding sites in the genome and have a characteristic chromatin structure. (Heinz et al., 2015). The number of potential enhancer elements greatly exceeds the number of coding regions, however most are maintained in a silent or poised state until an activating signal is received (Rada-Iglesias et al., 2011). Upon activation, binding of cell-type or temporal-specific transcription factors (TFs) to cognate DNA motifs recruits transcription co-activators, such as histone acetyltransferases CBP and p300 and RNA polymerase II (PolII) (Creyghton et al., 2010; Li et al., 2013). This results in two hallmarks of active enhancers: the production of bi-directional non-coding RNA transcripts known as enhancer RNAs (eRNAs) (Hah et al., 2011; Kim et al., 2010; Wang et al., 2011; Ørom et al., 2010) and elevated histone 3 lysine 27 acetylation (H3K27ac) (Creyghton et al., 2010).

Increasing evidence points to a direct role for eRNAs in enhancer function (Kim and Shiekhattar, 2015). eRNAs regulate looping between enhancers and promoters through recruitment of cohesin (Hsieh et al., 2014; Li et al., 2013), increase chromatin accessibility (Mousavi et al., 2013), and aid the recruitment of mediator to promoters (Lai et al., 2013). Consistently, depletion of eRNAs affects transcription from enhancer-associated genes (Kim et al., 2010; Lai et al., 2013; Li et al., 2013; Melo et al., 2013; Mousavi et al., 2013). At poised genes, eRNAs promote release of paused PolII into the gene body (Schaukowitch et al., 2014).

Several non-coding RNAs (ncRNAs) interact with chromatin-modifying enzymes and modulate enzymatic function (Cifuentes-Rojas et al., 2014; Di Ruscio et al., 2013; Kaneko et al., 2014a; 2014b; 2013; Wongtrakoongate et al., 2015; Yang et al., 2014). Binding of RNA to Polycomb repressive complex 2 (PRC2) decreases its methyltransferase activity and recruitment to promoters (Beltran et al., 2016; Cifuentes-Rojas et al., 2014; Kaneko et al., 2013; 2014a; 2014b). ncRNA transcribed proximal to the C/EBPA locus interacts with DNA methyltransferase 1 (DNMT1) to block DNA methylation at the promoter (Di Ruscio et al., 2013). A key question is whether eRNAs play a similar role in modulating chromatin at enhancers. Indeed, eRNA transcripts do not direct methylation changes at enhancers upon activation, which result from active transcription by PolII (Kaikkonen et al., 2013).

Elevated H3K27ac is another hallmark of active enhancers, produced by CBP and p300 (Jin et al., 2011; Tie et al., 2009). CBP/p300 bind a vast array of TFs through transactivation domains (TADs), acting as a transcription network 'hub' (Bedford et al., 2010; Wang et al., 2013). The broad interactome results in nearly-universal recruitment of CBP and p300 to enhancers, such that CBP/p300 occupancy is a key feature (Creyghton et al., 2010) and identifies enhancers genome-wide (May et al., 2012). The enzymatic activity of CBP and p300 is localized in their catalytic histone acetyltransferase (HAT) domain and targets both histones and numerous TF substrates, including p53 and PolII (Barlev et al., 2001; Jin et al., 2011; Schröder et al., 2013; Tie et al., 2009; Wang et al., 2008a). Acetylation of PolII by CBP promotes PolII release into the gene body (Schröder et al., 2013). H3K27ac correlates with regions of active transcription genome-wide (Tie et al., 2009; Wang et al., 2008b), and CBP-mediated acetylation can directly stimulate transcription by improving TF recruitment efficiency and promoter escape of PolII (Stasevich et al., 2014). Targeting the p300-HAT domain alone to enhancers using de-activated Cas9 nuclease (dCas9) and enhancer-specific guide RNAs (gRNAs) increases expression of enhancer-associated genes (Hilton et al., 2015). Thus, p300-mediated acetylation is sufficient for gene activation at endogenous enhancers and loci.

The localization of CBP activity at inappropriate enhancers is a critical factor in a subset of T-cell acute lymphoblastic leukemia (ALL). Somatic mutations create a new binding site for the transcription factor MYB upstream of the *Tal1* oncogene resulting in recruitment of CBP. This leads to increased H3K27ac and formation of a new enhancer element driving oncogenic *Tal1* expression (Mansour et al., 2014).

RNA could potentially impact the function of CBP and p300. Transcription of the antisense ncRNA khps1 from the promoter of the proto-oncogene SPHK1 helps to recruit p300 to the SPHK1 promoter (Postepska-Igielska et al., 2015). Moreover, stable depletion of eRNA transcribed from an enhancer for chorionic gonadotropin alpha (*Cga*) decreased H3K27ac (Pnueli et al., 2015). A key open question is whether there is a direct mechanistic connection between eRNA and CBP function at regulatory elements.

Here we demonstrate a direct interaction between CBP and RNA, including a large population of eRNAs. *In vivo* crosslinking and sequencing identified a subset of CBP-bound eRNAs associated with genes requiring CBP for their transcription. eRNA binding directly stimulates acetyltransferase activity of CBP *in vitro*, modulating H3K27ac levels. In cells, eRNA transcripts modulate their local chromatin environment, regulating H3K27ac to promote gene expression.

Results

CBP interacts with RNA *in vivo*

The ability of CBP to interact directly with RNA in cells is untested, although some evidence suggests interactions. First, in a high throughput survey in HeLa cells, p300 emerged as a candidate RNA binding protein (Castello et al., 2012). Second, p300 is associated with the antisense ncRNA Khps1 in native RIP-qPCR experiments (Postepska-Igielska et al., 2015). Third, CBP co-purifies with RNA after formaldehyde cross-linking of nuclei (G Hendrickson et al., 2016). Moreover, CBP contains a number of Zn^{2+} finger motifs and regions of predicted intrinsic disorder, both of which have been proposed to have RNA binding properties (Castello et al., 2012; Wang et al., 2013).

To validate the association of CBP with RNA without crosslinking, we carried out an RNA immunoprecipitation (RIP) experiment under native conditions from mouse embryonic fibroblasts (MEFs), and found that CBP IP co-purifies a population of bound RNA (Figure 1A, Figure S1A). To determine whether immunoprecipitated RNAs were interacting directly with CBP rather than indirectly through another CBP-bound protein, we used Photoactivatable ribonucleoside-enhanced crosslinking and immunoprecipitation (PAR-CLIP) (Figure 1B) (Hafner et al., 2010; Huppertz et al., 2014). We observed PAR-CLIP signal corresponding to CBP that was dependent on labeling of the bound RNA with 4-thiouridine (4-SU) (Figure 1C, Figure S1B-E). We note that, similar to other PAR-CLIP results (Hafner et al., 2010; Kaneko et al., 2013; 2014a), cross-linked CBP-RNA complexes migrated in a less defined band due to crosslinking with heterogeneous RNAs. Labeling was sensitive to RNase treatment, confirming that the material crosslinked to CBP was RNA (Figure 1E-F; S1F-H).

CBP-bound RNAs arise from sites of CBP binding

To investigate how CBP interacts with RNA across the genome, we sequenced CBP PAR-CLIP libraries from two biological replicates. To control for background RNA binding events (Friedersdorf and Keene, 2014), we also prepared libraries for nuclear-localized and Flag epitope-tagged GFP (nGFP) and for the DNA binding domain of the yeast TF Gal4p (Gal4-DBD) (two replicates each)

(Figure 2A, Figure S2A). Statistically enriched RNA regions were identified on individual and pooled replicate datasets using PARalyzer v1.1, which takes advantage of the T-to-C transitions caused by photo-crosslinking to identify interaction sites (Corcoran et al., 2011). CBP PAR-CLIP read densities from each replicate were well correlated in the RNA regions called by PARalyzer on the separate replicates (Pearson's coefficient = 0.93; Pearson's coefficient = 0.95 for common regions between replicates) (Figure S2B). Having confirmed the reproducibility of our CBP PAR-CLIP sequencing experiments, we pooled the replicates to identify a consensus set of CBP-bound RNA regions for downstream analyses. This resulted in 11,041 CBP-bound RNAs (CBP-RNAs) with a median size of 19bp (Figure S2C). There were 2367 bound RNAs in common between Gal4-DBD and nGFP controls, 2922 between CBP and Gal4-DBD, and 2020 between CBP and nGFP (Figure S2D–F); in total, ~71% (7,835) of CBP-RNAs did not appear in the background controls, suggesting that these represent specific signal from CBP-associated RNAs (Figure S2G, Table S1). We did not detect RNA-dependent interactions between CBP and other eRNA interacting proteins, such as Mediator (Lai et al., 2013) or NELF (Schaukowitch et al., 2014) under native (Figure S2H) or PAR-CLIP (Figure S2I) conditions. Using published ChIPseq data (Kagey et al., 2010; Sun et al., 2011), we found no difference in Med-1 signal at CBP-RNAs compared to background RNAs (Figure S2J), although NELF signal was enriched at CBP-RNAs, suggesting active transcription at these regions (Figure S2J). Thus, we were unable to detect co-binding of CBP and other eRNA interacting proteins to the same RNAs.

We compared the distribution of CBP PAR-CLIP signal with published CBP ChIPseq (Kasper et al., 2014) and GROseq (Meng et al., 2014) datasets in MEFs. Genome browser views of bound RNA regions and corresponding reads, such as at a target enhancer upstream of *Tet2* (Figure 2B-C), revealed increased PAR-CLIP read density. In many locations such as the *Tet2* enhancer, CBP PAR-CLIP reads mapped to regions of chromatin showing nascent transcription (by GROseq) and CBP occupancy (by ChIPseq; Figure 2B-C). The majority of CBP-RNAs (73%) were found in intergenic (47%) or intronic regions (26%) of the genome similar to CBP itself (72%; 43% intergenic, 29% intronic) (Figure 2D). The remaining CBP-RNAs arise from exons (23%) and very few (4%) from promoters (Figure 2D). As only 4% of CBP chromatin binding sites are at exons, we examined the distribution at exons and promoters in greater detail. The high level of exonic CBP-RNAs relative to CBP binding appears to result from increased false-positives due to the high transcription and stability of exons. First, actual PAR-CLIP reads are enriched at promoters and distal sites, compared to exons (Figure S2K). Second, the enrichment for CBP-RNAs at exons was relatively low, especially when compared to high transcription at exons (Figure S2K-L). Third, the TSS-1kb window used to define promoters limited the number of CBP-RNAs assigned to promoters. Therefore, the distribution of CBP-RNAs reflects patterns of CBP chromatin binding genome-wide.

Compared to RNAs bound in the negative control libraries, CBP-RNAs were enriched for CBP ChIPseq signal (Figure 2E) and were slightly more likely to comprise accessible chromatin (Figure 2F). CBP-RNAs had more nascent transcription by GROseq (Figure 2G), and were enriched for more stable RNA transcripts in total RNAseq data (Figure S2M). We then compared levels of nascent transcription (GROseq) to stable RNA transcripts (total RNAseq) at CBP-RNAs. The CBP-RNAs most enriched for GROseq reads also displayed high-read density in total RNAseq data (Figure S2N) and vice versa (Figure S2O). Nevertheless, CBP-RNAs with low enrichment in total RNAseq still demonstrated transcription by GROseq (Figure S2O, bottom deciles). Consistent with this, CBP-RNAs arising from stable transcripts at exons were strongly enriched for total RNAseq reads, but GROseq reads were strongly enriched at promoters and distal regions (Figure S2P). This reflects the ability of GROseq to detect the often-unstable, nascent RNA transcripts at these locations, where most CBP-RNAs arise (Figure 2D), and suggests that CBP-RNAs contain an

abundant population of nascent RNAs. There was an inverse correlation between peak-to-peak distance of CBP ChIPseq and PAR-CLIP signal when considering intersecting CBP and CBP-RNAs (Figure S2Q), with a higher Spearman co-efficient at short distances. Importantly, there was a consistent and more robust correlation with CBP ChIP signal for CBP-RNAs than for Gal4-DBD or nGFP control RNAs (Figure S2Q). Taken together these data demonstrate that CBP-RNAs localize at sites with nascent RNA transcription and within regions of chromatin bound by CBP.

CBP binds to eRNAs

As CBP-RNAs originated from transcribed chromatin regions occupied by CBP, two hallmarks of enhancers, we sought to determine whether CBP-RNAs corresponded to eRNAs. To account for the typical length of eRNAs, we focused on 1,138 locations where the center of the CBP-RNAs was less than 3.5kb from the nearest CBP peak and where CBP-ChIPseq and PAR-CLIP signal were strongly correlated (Figure S2Q) (De Santa et al., 2010; Kim et al., 2010). These CBP-RNAs close to CBP-ChIPseq peaks showed strong enrichment for PAR-CLIP reads (Figure S3A) compared to CBP-RNAs arising further from a CBP peak. They were also enriched for CBP ChIPseq and GROseq reads (Figure S3B-C), suggesting a positive relationship between PAR-CLIP signal and levels of CBP recruitment and transcription. To account for differences in CBP chromatin binding genome-wide (Figure 2D), we divided CBP peaks proximal to CBP-RNAs into promoter (TSS-1kb, 133 peaks, 13.5%), exonic (256 peaks, 26.2%) and distal (intergenic/intronic, 587 peaks 60.1%) sub groups (Figure 3A, Figure S3D). Sites with the highest enrichment for PAR-CLIP reads corresponded to regions most enriched for CBP in all three groups; the highest levels of CBP are found at the most enriched PAR-CLIP sites in promoter and distal regions - classical regions of CBP binding (Figure S3E). Locations with highest CBP binding (Figure S2F) and GROseq signal (Figure S3G) displayed the greatest enrichment for PAR-CLIP reads across all three groups. The distribution of reads across all three groups demonstrated slight enrichment for CBP binding at promoters and distal locations (Figure S3H-I), lower levels of transcription at distal sites (Figure S3J-K) but enrichment for PAR-CLIP reads at promoters and distal sites compared to exons (Figure S3L-M). The abundance of CBP-RNAs corresponded to the level of CBP chromatin binding at actively transcribed regions. Therefore, RNA binding to CBP appears to be locus-specific: CBP-RNAs arise from transcribed regions at locations where CBP binds to chromatin.

The large number of distal CBP-RNAs (Figure 2D) reflects the prevalence of CBP binding to enhancers in distal regions of the genome (Kasper et al., 2014). Active enhancers have high CBP occupancy and nascent transcription of eRNAs (Creyghton et al., 2010; Kim et al., 2010); our data suggests that these are also common features of CBP-RNA sites. Distal CBP-RNA sites display bi-directional RNA transcription, enriched CBP occupancy, more accessible chromatin (increased DNAse I hypersensitivity) and elevated levels of H3K27ac (Figure 3B). Furthermore, distal sites have higher H3K27ac (Figure S3N) and nascent transcription by GROseq (Figure S3O) compared to non-RNA interacting control CBP binding sites. Moreover, distal CBP-RNAs are enriched for H3K4me1 and depleted for H3K4me3, a characteristic profile of lysine methylation found at enhancers (Figure 3C-D) (Creyghton et al., 2010; Heintzman et al., 2007). CBP therefore appears to interact with eRNAs at distal enhancers (referred to hereafter as CBP-eRNA). We note that within CBP-eRNA loci, distal regions of strong GROseq signal are associated with elevated H3K4me3 (Figure 3A) reflecting more active transcription at these sites. We asked whether CBP-eRNAs had a chromatin signature of active enhancers, characterized by elevated H3K27ac. Of 766 CBP-RNAs intersecting H3K4me1, 532 (69.5%) also overlapped H3K27ac peaks (Figure 3E, Figure S3Q-S). However, of 533 distal CBP-eRNAs that intersect H3K4me1, 459 (86.1%) overlapped H3K27ac (Figure 3F, Figure S3P-R) and thus displayed an active enhancer signature.

Enhancers often regulate expression of adjacent genes (Kim et al., 2010; Lai et al., 2013; Li et al., 2013; Melo et al., 2013; Mousavi et al., 2013). Gene ontology (GO) analysis revealed that the genes nearest to CBP-eRNAs are significantly enriched for transcription regulators, including TFs, mediator subunits and epigenetic regulators (Figure S3S and Table S2). Furthermore, motif analysis identified binding sites for known CBP-interacting TFs (Table S3) (Bedford et al., 2010). The amount of CBP and p300 bound at promoters and enhancers is a poor predictor of the CBP/p300 requirement for expression of proximal genes (Kasper et al. 2014). Genes associated with CBP-eRNA (Table S4) tend to be downregulated upon CBP knockdown relative to genes not associated with CBP-eRNA (Figure S3T) (data from published microarray (Kasper et al., 2014)). We used RT-qPCR to examine the effect of CBP knockdown (control in Figure S3U) on newly identified eRNA transcripts and associated mRNA expression at a subset of genes (Figure 3G-H). The majority of tested mRNAs (8/9; 89%) were downregulated upon CBP knockdown (Figure 3H), and 4/8 (50%) of the corresponding eRNAs were also decreased (Figure 3G), indicating that these selected genes are direct targets of CBP. Overall, our data support the conclusion that distal CBP-eRNA regions represent a subset of active enhancers where eRNAs bind to CBP, and whose associated genes require CBP activity for expression.

In vitro reconstitution of CBP RNA binding

To investigate RNA binding to predicted RNA binding regions (RBRs) within CBP (BindN (Wang and Brown, 2006), Figure 4A, Figure S4A), we purified full length CBP (CBP-FL) from Sf9 cells (Figure S4B, left panel). Using an RNA pull-down (Bonasio et al., 2014) with *in vitro* transcribed RNA probes corresponding to eRNA-Klf6 (Figure 4B) and eRNA-Med13l (Figure 4C), we observed RNA interactions with CBP-FL (but not in control experiments), suggesting that CBP directly binds to RNA (Figure 4C-D, S4C-D).

RNA binding predictions for CBP (Figure 4A) suggested a highly basic region (residues 1561-1620) within the core HAT domain might contain the observed RNA binding activity. This region shares >90% identity with p300 and comprises 49 basic residues that are evolutionarily conserved and disordered (Delvecchio et al., 2013; Liu et al., 2008; Wang et al., 2008a; Yuan and Giordano, 2002). As highly basic and disordered regions are implicated in RNA binding (Castello et al., 2012; 2016; He et al., 2016), including RNA binding to epigenetic factors such as SCML2 and JARID2 (Bonasio et al., 2014; Kaneko et al., 2014a), we investigated the predicted RBR in the HAT domain. $CBP_{1196\text{-}1718}$ (CBP-HAT_{wt}), which contains all functional domains necessary for HAT activity (Delvecchio et al., 2013), was purified from bacteria (Figure S4B, right panel). RNA pull-down using sequences from nascent eRNAs (e-Klf6, e-Tet2, e-Klf4), processed lncRNAs (HOTAIR$_{1\text{-}300}$, Gas5, Meg3) and exonic RNAs (Id-1 (exon-1), Bbs2 (exon-1), Klf2 (exon-3)) (Figure 4E-F, Figure S4E-G), demonstrated that CBP-HAT_{wt} in isolation could bind to multiple different RNA sequences. However, we noted that binding to eRNA sequences was more consistent than binding to RNAs lncRNAs and exons (Figure S4G). Thus, CBP-HAT_{wt} recapitulated the interaction of CBP-FL with RNA (Figure 4B-D, Figure S4C-D), and displayed a general rather than sequence-specific RNA binding activity *in vitro*. As CBP-RNAs were enriched at sites of CBP chromatin binding (Figure 2), this supports a genomic locus-specific binding model, where RNAs transcribed proximal to CBP can bind to the RBR independent of RNA sequence.

Next, we used RNA electrophoretic mobility shift assays (EMSA) to evaluate RNA binding of CBP-HAT_{wt} to radiolabeled eRNA target sequences (Table S5). All sequences displayed a robust mobility shift when titrated with CBP-HAT_{wt} (Figure 4G-H, S4H, S4M, S4N). Moreover, binding to labeled eRNA-Mdm2 (Figure 4I) or eRNA-YY1 (Figure S4M: (iv)) was outcompeted by identical unlabeled eRNA probes. Importantly, single strand (ss) and double strand (ds) DNA with the same sequence could not compete with the CBP-eRNA interactions (Figure 4J), demonstrating that CBP-HAT_{wt} binds specifically to RNA *in vitro*.

The predicted RBR in the HAT domain (Q1559-K1608) (Figure S4A) forms a highly basic disordered loop which was proteolytically cleaved in available x-ray crystallographic structures of the p300 HAT domain (Delvecchio et al., 2013; Liu et al., 2008). Binding of eRNA-Klf6 to CBP in pull-downs (Figure 4E-F, Figure S4E) and eRNA-Mdm2 in EMSA (Figure 4K) was severely decreased when Q1559-K1608 was deleted (CBP-HAT$_{delta\text{-}loop}$) (Figure S4I). To test whether the charge of the loop was important for RNA binding, we mutated basic residues within the loop to acidic residues not predicted to interact with RNA (CBP-HAT$_{mutant\text{-}loop}$) (Figure S4I). We maintained lysine residues that are known targets for CBP mediated auto-acetylation regulating CBP-HAT activity and positively-charged residues important for lysine targeting by CBP (Liu et al., 2008; Thompson et al., 2001; 2004). Notably, the acetylation state of the RBR loop was important for RNA binding, as CBP-HAT$_{wt}$ only exhibited detectable RNA binding when co-expressed with lysine deacetylase ySir2 (Figure S4J), suggesting interplay between auto-acetylation of the RBR loop and RNA binding. In contrast, CBP-HAT$_{mutant\text{-}loop}$ displayed severe defects in RNA binding when co-expressed with ySir2, both in RNA pull-downs with eRNA-Klf6 (Figure 4E-F, Figure S4E) and in RNA EMSAs using radiolabelled eRNA probes (Figure 4L, Figure S4K), confirming the importance of basic residues within the RBR for RNA binding to the CBP-HAT domain.

We next asked whether CBP-eRNAs could interact with the identified RBR in CBP using PAR-CLIP in cells. We quantified binding of CBP-eRNA to full-length CBP$_{wt}$, CBP$_{delta\text{-}loop}$ or CBP$_{mutant\text{-}loop}$ in cells by PAR-CLIP followed by RT-qPCR (Figure 4M, control in Figure S4L). CBP$_{delta\text{-}loop}$ and CBP$_{mutant\text{-}loop}$ showed drastically reduced binding to CBP-eRNAs compared to CBP$_{wt}$ (Figure 4M), suggesting that the identified RBR within the regulatory loop is the predominant but not the only site of interaction for CBP with eRNAs. Overall, the *in vitro* RNA binding experiments demonstrate that CBP can directly associate with RNA. Moreover, a specific RNA-binding sequence located within a basic loop that is part of the HAT domain, constitutes a previously unrecognized RBR within CBP. The binding data suggest that CBP can bind to RNA in a locus-specific manner, independent of RNA sequence; thus a bias towards eRNAs is observed due to the high recruitment of CBP to enhancer regions where it interacts with nascent eRNA transcripts.

CBP acetyltransferase activity is stimulated by RNA binding

Having defined an RBR within the HAT domain of CBP, we next investigated whether RNA binding affects the HAT activity of CBP, using a radioactive filter-binding assay (Figure S5A). Increasing concentrations of two different eRNAs, eRNA-Ccnd1 and eRNA-Klf6, stimulated CBP HAT activity (Figure 5A). Both eRNAs stimulated activity in a dose dependent manner, but the magnitude and pattern of activity differed slightly between eRNA species. There was no equivalent stimulation when titrating control Ccnd1 ssDNA or dsDNA (Figure 5A). Stimulation was independent of RNA sequence, but required RNA binding to the RBR: HOTAIR$_{1\text{-}300}$ and Id-1 (exon-1), which bound robustly to CBP-HAT$_{wt}$ (Figure S5B) stimulated activity, but Meg3, which bound poorly, did not (Figure S5B-C). Importantly, HAT activity did not increase in CBP deleted for the RBR (CBP-HAT$_{delta\text{-}loop}$, Figure 5B). Thus, RNA binding to the RBR within the HAT domain of CBP stimulates HAT activity.

Next, we determined whether RNA binding increases CBP-dependent histone modifications. CBP acetylates distinct lysine residues, including H3K27ac and H3K18ac on histone H3 and H4K5ac on histone H4 *in vitro* (Henry et al., 2013). We repeated the HAT assay using reconstituted recombinant nucleosomes (Figure S5D) and assayed by western blot. The level of both H3K27ac and H4K5ac increased as eRNA concentration was titrated (Figure 5C-E, Figure S5E-G), confirming that increased activity with RNA translates to higher H3K27ac (Figure 5C) and H4K5ac (Figure 5D) *in vitro*. Stimulation was independent of RNA sequence; eRNA-YY1 (Figure 5E), eRNA-Mdm2, eRNA-Ccnd1 and lncRNA-HOTAIR$_{1\text{-}300}$ all stimulated both H3K27ac and H4K5ac

(Figure S5E-G), although the different sequences generated different profiles of acetylation. The effect was also observed for recombinant H3 in isolation (Figure S5H, quantified in Figure S5I). The dose response is U-shaped; at high molar ratios of RNA to CBP-HAT there was a drop in H3K27ac (Figure 5C, Figure S5I) and H4K5ac (Figure 5D), which could result from CBP interactions with RNA outside of the primary CBP-RBR at high RNA concentrations. Consistent with this hypothesis, the activity of CBP-HAT$_{delta\text{-}loop}$ also decreased at high RNA concentrations (Figure 5B); we note that most eRNAs have low abundance in different systems (Kim et al., 2010; Lam et al., 2013; Li et al., 2013). When the experiment was repeated with recombinant human MOF (hMOF) there was no stimulation of H4K16ac, the major acetylation site of hMOF (Figure S5J). MYST-type acetyltransferases such as hMOF, although also regulated by acetylation, do not contain a CBP/p300-like RBR (Wang et al., 2008a; Yuan et al., 2012).

Our data demonstrate that RNA binding to the HAT domain of CBP, through the identified RBR, stimulates the acetyltransferase activity of CBP in an RNA concentration-dependent manner, generating increased levels of H3K27ac and H4K5ac *in vitro*.

Mechanism of RNA stimulation of acetyltransferase activity

CBP/p300 display a unique mechanism of regulation among acetyltransferase families whereby a basic activation loop within the HAT domain acts as a pseudo-substrate, binding to the active site and auto-inhibiting HAT activity by preventing substrate binding (Liu et al., 2008; Thompson et al., 2004; Wang et al., 2008a). Acetylation of the activation loop results in its displacement, thus allowing substrate binding to the active site. In steady-state HAT assays, a loss of auto-inhibition is observed as a decrease in the concentration of substrate needed to reach half maximum acetylation rate (K_m) (Thompson et al., 2004). Remarkably, the location of the CBP/p300 activation loop largely overlaps the position of the RBR within the HAT domain (Figure 4A, Figure S4A). We therefore tested whether eRNA binding to the RBR could stimulate the HAT activity of CBP through a similar reduction of auto-inhibition.

We adapted our radioactive filter binding assay to evaluate the steady-state kinetic mechanism of stimulation of CBP activity by eRNA (Bowers et al., 2010) (Figure 5F-G; kinetic parameters are summarized in Figure S5K and a model for activation in Figure 5J). Our calculated value of $K_{m(H3\text{-}1\text{-}21)}$ for CBP-HAT$_{wt}$ ($K_{m(H3\text{-}1\text{-}21)}$= 44.55 +/- 3.99 uM) (Figure 5F) closely matches previous values for recombinant p300 HAT domain ($K_{m(H4\text{-}15)}$ = 40 +/- 8 uM) (Thompson et al., 2004). Consistent with our model, addition of 10nM eRNA-Mdm2 decreased the $K_{m(H3\text{-}1\text{-}21)}$ of CBP-HAT$_{wt}$ from 44.55 +/- 3.99 to 26.42 +/- 3.55uM (Figure 5F). We note that while 10nM eRNA also slightly decreased the K_{cat} (Figure 5F), the specificity constant K_{cat}/K_m was increased, reflecting an increase in catalysis (Figure 5H). Hence, in common with acetylation of the activation loop, the stimulation of CBP HAT activity by eRNA binding is due to its increased affinity for histone substrate rather than to an alteration of the catalytic mechanism.

To confirm this mechanism, CBP-HAT$_{mutant\text{-}loop}$, which does not bind to eRNA (Figure 4N), displayed no change in the K_m with 10nM eRNA (Figure 5G). Indeed, the K_m of CBP-HAT$_{mutant\text{-}loop}$ in the absence of eRNA was already decreased ($K_{m(H3\text{-}1\text{-}21)}$= 27.30 +/-5.65 uM) compared to CBP-HAT$_{wt}$ ($K_{m(H3\text{-}1\text{-}21)}$= 44.55 +/- 3.99 uM) (Figure S5K). This indicates that mutation of basic residues to acidic residues within the loop is sufficient to displace the loop from the active site and thus mimic the effect of eRNA binding. Inclusion of eRNA, which does not interact with the mutant loop, has no further effect on the K_m and consequently there is no increase in $K_{cat}/K_{m(H3\text{-}1\text{-}21)}$ (Figure 5I, Figure S5K). Importantly, K_{cat} with 10nM RNA was similar for both CBP-HAT$_{mutant\text{-}loop}$ and CBP-HAT$_{wt}$, which suggested that the decrease in K_{cat} observed in both cases was independent of eRNA binding to the RBR (compare Figures 5F and 5G, values in Figure S5K). However, as 10nM

RNA did not change the K_m of CBP-$HAT_{mutant\text{-}loop}$, the specificity constant K_{cat}/K_m was slightly decreased (Figure 5I, Figure S5K). These data indicate that eRNA binding to the RBR within the activation-loop results in its displacement from the active site of CBP. This allows improved substrate binding, decreases the K_m in the presence of eRNA, and thus enhances the HAT activity of CBP (see model in Figure 5J).

eRNAs modulate the acetyltransferase activity of CBP *in vivo*

Our data demonstrate that CBP binds to RNAs transcribed close to CBP binding sites such as at the *YY1* enhancer (Figure 6A); recruitment of CBP to active enhancers results in binding to eRNAs, and that eRNA binding to the HAT domain of CBP stimulates its acetyltransferase activity.

We next asked whether depletion of CBP-eRNAs in cells reduces histone acetylation in a locus-specific manner. Depletion of eRNA transcripts can specifically reduce expression of mRNA regulated by the target enhancer (Kim et al., 2010; Lai et al., 2013; Li et al., 2013). RT-qPCR following transfection of antisense-oligonucleotides (ASO) targeting eRNA-YY1 (Figure 6A, Figure S6A), compared to GFP ASO control, revealed specific depletion of the targeted eRNA-YY1 and reduction of the adjacent coding mRNA (Figure 6B, Figure S6E). Importantly, eRNA and mRNA at non-targeted *Ccnd1* loci (Figure 6B, bottom panel; Figure S6E) was not significantly reduced upon depletion of eRNA-YY1. We note that eRNA-YY1 depletion also slightly affects expression of *Tet2* mRNA, likely indirectly through depletion of YY1 protein, as the *Tet2* promoter contains a YY1 motif (TRANSFAC, (Matys et al., 2006)). Similarly, ASO that depleted eRNA-Ccnd1 (Figure S6B) reduced levels of eRNA and adjacent coding mRNA at *Ccnd1*, but not at non-targeted *YY1* and *Tet2* loci (Figure 6C, Figure S6E).

We depleted eRNA-YY1 and found a similar reduction of H3K27ac (Figure 6D) and H3K18ac (Figure 6E), whereas there was no significant change in acetylation at the *Ccnd1* control enhancer and promoter loci (Figure 6D-E, bottom panel) or at *Tet2* control loci (Figure S6F-G, bottom panel). There was also no change in CBP occupancy at enhancer or promoter regions (Figure 6F). Similarly, depletion of eRNA-Ccnd1 decreased H3K27ac (Figure 6G) and H3K18ac (Figure 6H) at the *Ccnd1* enhancer and promoter, but produced no change in acetylation at the *YY1* enhancer and promoter (Figure 6G-H, bottom panels) and no change in CBP occupancy (Figure 6I). Acetylation was also reduced at the *Tet2* enhancer and promoter upon depletion of eRNA-Tet2 (Figure S6H-I), with no alteration in CBP binding (Figure S6J) or acetylation at *YY1* control loci. (we note that this did not lead to decreased *Tet2* mRNA, consistent with our previous observation that loss of CBP did not reduce *Tet2* mRNA levels in Figure 3H). Importantly, for all three examples, eRNA depletion caused decreased acetylation specifically at the target enhancer and promoter, but not at control enhancer and promoter loci.

Our findings lead to a model (Figure 7) where CBP binding to specific eRNA transcripts regulates CBP acetyltransferase activity in *cis*. This results in a local increase in CBP-dependent histone acetylation at the same enhancer and target promoter regions. eRNA binding therefore contributes to enhancer-specific patterns of histone acetylation at regulatory regions.

Discussion

Our results provide direct evidence of RNA binding to CBP in cells. We show that CBP interacts in a locus-specific manner with RNAs transcribed proximal to sites of CBP chromatin binding. By interacting with a CBP/p300-specific RBR located within its catalytic HAT domain, RNA stimulates the HAT activity of CBP. This observation has particular importance at enhancers, where CBP binding, histone acetylation, and eRNA production are interconnected. Localizing acetyltransferase activity to enhancers is sufficient to promote transcription of associated genes (Hilton et al., 2015).

Our findings link these events in a mechanistic manner: eRNA binding to CBP in *cis* stimulates the localized acetyltransferase activity at enhancers, increasing H3K27ac and H3K18ac at the enhancer and, importantly, at the target promoter, thereby promoting gene expression. Nevertheless, further work is needed to fully elucidate the role of CBP dependent acetylation at enhancers in regulating gene expression.

The mechanism of regulation by activation loop is unique to CBP/p300 among acetyltransferases (Wang et al., 2008a). Remarkably, we show that this same motif renders the HAT activity of CBP sensitive to RNA (Figure 5F-G). This feature may be unique to CBP/p300, as the activity of the acetyltransferase hMOF was not affected by RNA (Figure S5J). Our observation that acetylation was important for RNA binding (Figure S4K) suggests a possible interplay between RNA binding and auto-acetylation of the loop region. Moreover, CBP activity is also sensitive to interactions with transcription factor binding partners (Chen et al., 2001; Perissi et al., 1999). Direct binding of ncRNAs to the chromatin modifying enzymes PRC2 (Cifuentes-Rojas et al., 2014; Kaneko et al., 2014b), and DNMT1 (Di Ruscio et al., 2013) modulate their function. Our data adds CBP to the list of enzymes whose function is modified by RNA binding, and we demonstrate that eRNA in particular contributes to an active chromatin profile through stimulation of CBP HAT activity in *cis*.

Our data suggests that RNA binding to CBP could be similar to PRC2 in using a promiscuous binding model, defined as the ability to bind to many RNA sequences with broadly similar affinities (Cifuentes-Rojas et al., 2014; Davidovich et al., 2015; Kaneko et al., 2013; 2014a). RNA binding to CBP also appears to be locus-specific: CBP binds to RNAs where it is recruited to chromatin. CBP bound at promoters may therefore also be regulated by interactions with RNA, although the prevalence of enhancer bound CBP (Kasper et al., 2014) results in a strong bias towards eRNA binding. Promiscuous, locus-specific RNA binding has obvious benefits for a transcriptional co-activator such as CBP with a broad genome-wide binding profile, allowing RNAs to stimulate local CBP activity regardless of their sequence. Moreover, variations in binding between RNAs could generate locus-specific activity and acetylation profiles, thus enabling fine-tuning of target gene expression. This model enables a de-coupling of CBP/p300 recruitment from histone acetylation and transcriptional output, helping to explain why CBP/p300 recruitment is a poor predictor of gene activation (Bedford et al., 2010; Kasper et al., 2014). Consistently, depletion of CBP-eRNAs decreased H3K27ac and H3K18ac specifically at associated promoters and modulated gene expression (Figure 6F-G, I-J).

In conclusion, we show that RNAs transcribed proximal to CBP binding sites directly interact with CBP in *cis*. Binding to the RBR within the catalytic HAT domain of CBP – a region critical for regulating HAT activity - allows substrate to bind more easily and thereby stimulates the HAT activity of CBP. At active enhancers, CBP binds to eRNAs leading to elevated histone acetylation and increased transcription of target genes (Figure 7). In this model, CBP-mediated histone acetylation can be regulated independently from CBP recruitment, and allows enhancer- and gene-specific tuning of acetylation. By stimulating CBP activity, RNA binding can generate a tailored chromatin environment at target genes to fine-tune transcriptional output.

Accession Numbers

The GEO repository series accession number for the CBP PAR-CLIP and background control (yeast Gal4-DBD and nls-GFP) PAR-CLIP datasets, as well as read density profiles for CBP-PAR-CLIP is GSE75684.

Author Contributions

Study was conceived by SLB and DB. SLB and DB initiated and led the study with input from RB, RS and DR. DB, SLB, RB and RS designed experiments. DB carried out all experiments. DB and GD analyzed high-throughput sequencing data. DB, SLB and RB wrote the manuscript. All authors reviewed and commented on the manuscript.

Acknowledgments

We thank P. Brindle and L. Kasper for *CBP/p300 flox/flox* MEFs. R. Marmorstein for hMOF; C. He for Meg3 RNA; H.Goodarzi for advice on RNA motifs. J. Chen for experiments not included in the manuscript. H.Fan lab for advice and equipment. R. Marmorstein, D.Schultz and J. Dorsey for advice on experiments. P.Sen, P.Shah, M.Sammons and A.Twelvetrees provided considerable support, advice and critical reading of the manuscript. SLB is supported by NIH grant R01 CA078831. RB was supported by an NIH Innovator Award (DP2MH107055), the Searle Scholars Program (15-SSP-102), the March of Dimes Foundation (1-FY-15-344), and the W.W. Smith Charitable Trust (C1404).

Figure legends

Figure 1: CBP interacts with RNA in vivo

A) Native RNA-IP of CBP. Top, RNA immunprecipitated with CBP was purified and imaged with SYBR gold. Bottom, western blot for CBP.
B) Schematic of PAR-CLIP protocol. 4-Thiouridine (4-SU).
C) CBP PAR-CLIP required 4-SU: top, autoradiography; bottom, western blot for CBP on PAR-CLIP membrane.
D) Quantification of CBP PAR-CLIP. Error bars represent mean +/- s.e.m; n=4.
E) CBP PAR-CLIP signal was sensitive to RNAse. 1x RNAse cocktail contained: RNAse A (0.01mU/ul) + RNase T1 (0.4mU/ul).
F) Quantification of RNase titration. Error bars represent mean +/- s.e.m; n=4; *P*-values from two-tailed Student's t-test: *P< 0.05; **P< 0.01; ***P< 0.001.

Figure 2: CBP-RNAs arise at regions of CBP enrichment.

A) Autoradiography of CBP PAR-CLIP and nls-GFP (nGFP) and yeast Gal4 DNA binding domain (Gal4-DBD) background control. Membrane excised for library preparation (Dashed box).
B) UCSC genome browser view of CBP-RNA upstream of the Tet2 promoter. Top; GROseq signal (+ strand purple, - strand grey); CBP-RNA (PARalyzer) orange bars; 2 replicates PAR-CLIP reads (orange/purple); CBP peaks (blue bars); 2 replicates CBP reads (light blue/dark blue).
C) Close-up of box from G). Sense strand (s) and antisense strand (as)
D) Distribution of CBP and CBP-RNA by genome region (Promoter = 1kb upstream of TSS).
E-G) Read density over CBP-RNAs and enriched control RNAs. CBP peaks were randomly downsampled to match the size of the background dataset (5581); F) CBP ChIPseq signal (GSE54453, (Kasper et al., 2014)); G) DNaseI hypersensitivity (ENCODE, GSE37074); H) GROseq (GSM1524922, (Meng et al., 2014)). *P*-values from Mann-Whitney U-test.

Figure 3: CBP binds to eRNAs and directs gene expression from CBP-eRNA enhancers

A) Heatmaps of RNA bound CBP peaks (<3.5kb). CBP peaks were categorized into Promoter (TSS-1kb), Exon and Distal (Intronic/Intergenic). Heat maps show +/- 2.5kb window from centre of CBP peak, reads were binned over 50bp.
B) UCSC genome browser views of CBP-eRNA regions proximal to *Klf6, Sp3, Med13l, Yy1, Ccnd1* and *Tet2* genes. Top; GROseq signal (Sense, purple; antisense, grey); CBP-RNAs (PARalyzer) orange bars; 2 replicates PAR-CLIP reads (orange/purple); CBP peaks (blue bars); 2 replicates CBP reads (light blue/dark blue); H3K27ac reads (green). Sense strand (s) and antisense strand (as) directions are indicated.
C-D) Reads at CBP-RNAs sorted by genome region: C) H3K4me3; D) H3K4me1. *P*-values from Mann-Whitney U-test.
E-F) Venn diagrams show CBP ChIPseq peaks with H3K4me1 intersecting H3K27ac for: E) CBP-RNAs; F) CBP-eRNAs. *P*-values from permutation test with random regions restricted to TSS-40kb.
G-H) RT-qPCR of G) CBP-eRNAs. Strand is indicated (s=sense, as=antisense); and H) Nearest gene. Data show $\log_2$ fold change between control adenoviral GFP (Adv-GFP, green) or knockdown with adenoviral Cre (Adv-Cre, purple); n=3.

Figure 4: *In vitro* reconstitution of CBP RNA binding

A) CBP domains and RNA binding prediction (BindN). Non-binding residues (green) and binding residues (red) are indicated. Magnified sequence shows strong predicted RNA binding region in the CBP-HAT_{wt} domain.

B-C) *In vitro* pull down of B) eRNA-Klf6$_s$ and C) eRNA-Med13l$_s$. s=sense, as=antisense strand RNA. Replicate images in Figure S4C-D.
D) Quantification of RNA-pulldown data in B-C. n=3.
E) *In vitro* pull down of eRNA-Klf6$_s$. RNA Input and protein fractions in Figure S4E).
F) Quantification of RNA-pulldown data in B-C. n=3.
G-H) RNA EMSA of eRNA probes using CBP-HAT$_{wt}$. G) eRNA-Mdm2$_s$; H) eRNA-Med13l$_s$. Replicate images in Figure S4M; whole gel images in Figure S4N.
I-J) Competition binding RNA EMSAs. Binding of 2nM ^{32}-P radiolabelled eRNA-Mdm2 to CBP-HAT$_{wt}$ (2000nM) was competed with: I) 0-20nM unlabelled eRNA-Mdm2; J) 1nM, 10nM and 20nM un-labeled eRNA-Mdm2 (RNA), dsDNA or ssDNA with the same sequence.
K) RNA EMSA using CBP-HAT$_{delta\text{-}loop}$. eRNA-Med13l was titrated with 0-8000nM CBP-HAT$_{delta\text{-}loop}$. (*) CBP-HAT$_{wt}$ (2000nM).
L) RNA EMSA using CBP-HAT$_{mutant\text{-}loop}$. eRNA-Med13l was titrated with 0-8000nM CBP-HAT$_{mutant\ loop}$. (*) CBP-HAT$_{wt}$ (2000nM).
M) RBR mediates RNA binding to FL-CBP *in vivo*. PAR-CLIP for GFP-tagged CBP$_{wt}$, CBP$_{delta\text{-}loop}$ or CBP$_{mutant\text{-}loop}$ in MEFs was followed by RT-qPCR for eRNA-Ccnd1, eRNA-Tet2, eRNA-YY1, eRNA-Klf6. Control lncRNA Malat-1 was not identified by PARalyzer v1.1. *P*-values from two-tailed Student's t-test: *P< 0.05; **P< 0.01; ***P< 0.001.

Figure 5: CBP acetyltransferase activity is stimulated by RNA binding

A) RNA stimulated CBP HAT activity in filter binding assays. 5nM CBP-HAT$_{wt}$ was titrated with 0-40nM eRNA (eRNA-Ccnd1 and eRNA-Klf6) or control (dsDNA/ssDNA with same sequence). Data shows fold change in rate (V_{max}/[E], (s^{-1})) from 0nM RNA. Shaded regions show mean +/- s.e.m (RNA n=3, control n=1). s=sense, as=antisense strand RNA.
B) Stimulation of CBP HAT activity required the RBR. 1nM CBP-HAT$_{wt}$ or CBP-HAT$_{delta\text{-}loop}$ was titrated with 0-40nM eRNA-Mdm2. Shaded regions show mean +/- s.e.m (n=4).
C-E) Western blot HAT assay using recombinant nucleosome substrate. 1nM CBP-HAT$_{wt}$ was titrated with 0-10nM eRNA-YY1$_{as}$. RNA stimulated: C) H3K27ac (H3 normalized) and; D) H4K5ac (H4 normalized). E) Western blot for H3K27ac, H4K5ac and H3/H4. Coomassie (bottom panel) shows individual histones.
F-G) Steady state filter binding assay. Michaelis-Menten plots for: F) CBP-HAT$_{wt}$; G) CBP-HAT$_{mutant\text{-}loop}$. Reactions contained 0nM (green) or 10nM (orange) eRNA-Mdm2. Concentrations of CBP-HAT domain and Acetyl-CoA were 10nM and 100uM respectively. H3-1-21 peptide from 0-200uM (n=4). Derived kinetic parameters for K_m and K_{cat} in Figure S5K.
H-I) Specificity constant ($K_{cat}/K_{m(H3\text{-}1\text{-}21)}$) for reaction with 0nM or 10nM eRNA-Mdm2. H) CBP-HAT$_{wt}$; I) CBP-HAT$_{mutant\text{-}loop}$.
J) Mechanism for stimulation of CBP-HAT activity by RNA binding.

Figure 6: Localized eRNA binding can stimulate acetyltransferase activity of CBP in vivo

A) UCSC genome browser of YY1 enhancer and promoter regions. Colours as in Figure 2B.
B-C) Depletion of PAR-CLIP eRNA using antisense olignucleotide (ASO) targeting: B) eRNA-YY1$_{antisense}$ (purple); and C) eRNA-Ccnd1$_{sense}$ (blue); GFP-control (green). RT-qPCR shows fold-change in eRNA and associated mRNA at targeted gene (top) or non-targeted control gene (bottom). Error bars represent mean +/- s.e.m; n=4.
D-F) ChIP-qPCR at enhancer and promoter regions following ASO depletion of eRNA-YY1 (purple) or GFP-control (green). Foldchange (IP/H3) for: D) H3K27ac; E) H3K18ac and F) CBP (IP/Input) at *YY1* and non-targeted control gene *Ccnd1* (bottom). Error bars represent mean +/- s.e.m; n=4.
G-I) ChIP-qPCR at enhancer and promoter regions following ASO depletion of eRNA-Ccnd1 (blue) or GFP-control (green). Foldchange (IP/H3) for: G) H3K27ac; H) H3K18ac and I) CBP (IP/Input) at

Ccnd1 and non-targeted control gene *YY1* (bottom). Error bars represent mean +/- s.e.m; n=4. *P*-values from two-tailed Student's t-test: *P< 0.05; **P< 0.01; ***P< 0.001.

Figure 7: Model for RNA stimulation of CBP HAT activity during enhancer activation.
i) At inactive enhancers, CBP activity is limited by the activation loop, which occupies the active site.
ii) During activation, recruitment of PolII by bound TFs PolII results in eRNA transcription.
iii) eRNAs bind to the CBP HAT domain RBR, displacing the activation loop, stimulating the HAT activity of CBP and increasing H3K27ac at the enhancer and associated promoter.

References

Bailey, T.L., and Elkan, C. (1994). Fitting a mixture model by expectation maximization to discover motifs in biopolymers. Proc Int Conf Intell Syst Mol Biol *2*, 28–36.

Barlev, N.A., Liu, L., Chehab, N.H., Mansfield, K., Harris, K.G., Halazonetis, T.D., and Berger, S.L. (2001). Acetylation of p53 activates transcription through recruitment of coactivators/histone acetyltransferases. Mol Cell *8*, 1243–1254.

Bedford, D.C., Kasper, L.H., Fukuyama, T., and Brindle, P.K. (2010). Target gene context influences the transcriptional requirement for the KAT3 family of CBP and p300 histone acetyltransferases. Epigenetics *5*, 9–15.

Beltran, M., Yates, C.M., Skalska, L., Dawson, M., Reis, F.P., Viiri, K., Fisher, C.L., Sibley, C.R., Foster, B.M., Bartke, T., et al. (2016). The interaction of PRC2 with RNA or chromatin is mutually antagonistic. Genome Res *26*, 896–907.

Berndsen, C.E., and Denu, J.M. (2005). Assays for mechanistic investigations of protein/histone acetyltransferases. Methods *36*, 321–331.

Bezzi, M., Teo, S.X., Muller, J., Mok, W.C., Sahu, S.K., Vardy, L.A., Bonday, Z.Q., and Guccione, E. (2013). Regulation of constitutive and alternative splicing by PRMT5 reveals a role for Mdm4 pre-mRNA in sensing defects in the spliceosomal machinery. Genes Dev *27*, 1903–1916.

Bonasio, R., Lecona, E., Narendra, V., Voigt, P., Parisi, F., Kluger, Y., and Reinberg, D. (2014). Interactions with RNA direct the Polycomb group protein SCML2 to chromatin where it represses target genes. Elife *3*, e02637.

Bowers, E.M., Yan, G., Mukherjee, C., Orry, A., Wang, L., Holbert, M.A., Crump, N.T., Hazzalin, C.A., Liszczak, G., Yuan, H., et al. (2010). Virtual ligand screening of the p300/CBP histone acetyltransferase: identification of a selective small molecule inhibitor. Chem Biol *17*, 471–482.

Castello, A., Fischer, B., Eichelbaum, K., Horos, R., Beckmann, B.M., Strein, C., Davey, N.E., Humphreys, D.T., Preiss, T., Steinmetz, L.M., et al. (2012). Insights into RNA biology from an atlas of mammalian mRNA-binding proteins. Cell *149*, 1393–1406.

Castello, A., Fischer, B., Frese, C.K., Horos, R., Alleaume, A.-M., Foehr, S., Curk, T., Krijgsveld, J., and Hentze, M.W. (2016). Comprehensive Identification of RNA-Binding Domains in Human Cells. Mol Cell *63*, 696–710.

Chen, C.-J., Deng, Z., Kim, A.Y., Blobel, G.A., and Lieberman, P.M. (2001). Stimulation of CREB Binding Protein Nucleosomal Histone Acetyltransferase Activity by a Class of Transcriptional Activators. Mol Cell Biol *21*, 476–487.

Cifuentes-Rojas, C., Hernandez, A.J., Sarma, K., and Lee, J.T. (2014). Regulatory Interactions between RNA and Polycomb Repressive Complex 2. Mol Cell *55*, 171–185.

Corcoran, D.L., Georgiev, S., Mukherjee, N., Gottwein, E., Skalsky, R.L., Keene, J.D., and Ohler, U. (2011). PARalyzer: definition of RNA binding sites from PAR-CLIP short-read sequence data. Genome Biol *12*, R79.

Creyghton, M.P., Cheng, A.W., Welstead, G.G., Kooistra, T., Carey, B.W., Steine, E.J., Hanna, J., Lodato, M.A., Frampton, G.M., Sharp, P.A., et al. (2010). Histone H3K27ac separates active from poised enhancers and predicts developmental state. Pnas *107*, 21931–21936.

Davidovich, C., Wang, X., Cifuentes-Rojas, C., Goodrich, K.J., Gooding, A.R., Lee, J.T., and Cech, T.R. (2015). Toward a consensus on the binding specificity and promiscuity of PRC2 for RNA. Mol Cell *57*, 552–558.

1228 Davidovich, C., Zheng, L., Goodrich, K.J., and Cech, T.R. (2013). Promiscuous RNA binding by
1229 Polycomb repressive complex 2. Nat Struct Biol *20*, 1250–1257.

1230 De Santa, F., Barozzi, I., Mietton, F., Ghisletti, S., Polletti, S., Tusi, B.K., Muller, H., Ragoussis, J.,
1231 Wei, C.-L., and Natoli, G. (2010). A large fraction of extragenic RNA pol II transcription sites
1232 overlap enhancers. PLoS Biol *8*, e1000384.

1233 Delvecchio, M., Gaucher, J., Aguilar-Gurrieri, C., Ortega, E., and Panne, D. (2013). Structure of
1234 the p300 catalytic core and implications for chromatin targeting and HAT regulation. Nat Struct
1235 Biol.

1236 Di Ruscio, A., Ebralidze, A.K., Benoukraf, T., Amabile, G., Goff, L.A., Terragni, J., Figueroa, M.E.,
1237 De Figueiredo Pontes, L.L., Alberich-Jorda, M., Zhang, P., et al. (2013). DNMT1-interacting RNAs
1238 block gene-specific DNA methylation. Nature *503*, 371–376.

1239 Dignam, J.D., Lebovitz, R.M., and Roeder, R.G. (1983). Accurate transcription initiation by RNA
1240 polymerase II in a soluble extract from isolated mammalian nuclei. Nar *11*, 1475–1489.

1241 Friedersdorf, M.B., and Keene, J.D. (2014). Advancing the functional utility of PAR-CLIP by
1242 quantifying background binding to mRNAs and lncRNAs. Genome Biol *15*, R2.

1243 G Hendrickson, D., Kelley, D.R., Tenen, D., Bernstein, B., and Rinn, J.L. (2016). Widespread RNA
1244 binding by chromatin-associated proteins. Genome Biol *17*, 28.

1245 Gagnon, K.T., and Maxwell, E.S. (2011). Electrophoretic mobility shift assay for characterizing
1246 RNA-protein interaction. Methods Mol Biol *703*, 275–291.

1247 Gupta, S., Stamatoyannopoulos, J.A., Bailey, T.L., and Noble, W.S. (2007). Quantifying similarity
1248 between motifs. Genome Biol *8*, R24.

1249 Hafner, M., Landthaler, M., Burger, L., Khorshid, M., Hausser, J., Berninger, P., Rothballer, A.,
1250 Ascano, M., Jungkamp, A.-C., Munschauer, M., et al. (2010). Transcriptome-wide identification of
1251 RNA-binding protein and microRNA target sites by PAR-CLIP. Cell *141*, 129–141.

1252 Hah, N., Danko, C.G., Core, L., Waterfall, J.J., Siepel, A., Lis, J.T., and Kraus, W.L. (2011). A
1253 rapid, extensive, and transient transcriptional response to estrogen signaling in breast cancer cells.
1254 Cell *145*, 622–634.

1255 He, C., Sidoli, S., Warneford-Thomson, R., Tatomer, D.C., Wilusz, J.E., Garcia, B.A., and Bonasio,
1256 R. (2016). High-Resolution Mapping of RNA-Binding Regions in the Nuclear Proteome of
1257 Embryonic Stem Cells. Mol Cell *64*, 416–430.

1258 He, H.H., Meyer, C.A., Shin, H., Bailey, S.T., Wei, G., Wang, Q., Zhang, Y., Xu, K., Ni, M., Lupien,
1259 M., et al. (2010). Nucleosome dynamics define transcriptional enhancers. Nat Genet *42*, 343–347.

1260 Heintzman, N.D., Stuart, R.K., Hon, G., Fu, Y., Ching, C.W., Hawkins, R.D., Barrera, L.O., Van
1261 Calcar, S., Qu, C., Ching, K.A., et al. (2007). Distinct and predictive chromatin signatures of
1262 transcriptional promoters and enhancers in the human genome. Nat Genet *39*, 311–318.

1263 Heinz, S., Romanoski, C.E., Benner, C., and Glass, C.K. (2015). The selection and function of cell
1264 type-specific enhancers. Nat Rev Mol Cell Biol *16*, 144–154.

1265 Henry, R.A., Kuo, Y.-M., and Andrews, A.J. (2013). Differences in specificity and selectivity
1266 between CBP and p300 acetylation of histone H3 and H3/H4. Biochemistry *52*, 5746–5759.

1267 Hilton, I.B., D'Ippolito, A.M., Vockley, C.M., Thakore, P.I., Crawford, G.E., Reddy, T.E., and
1268 Gersbach, C.A. (2015). Epigenome editing by a CRISPR-Cas9-based acetyltransferase activates
1269 genes from promoters and enhancers. Nat Biotechnol *33*, 510–517.

Hsieh, C.-L., Fei, T., Chen, Y., Li, T., Gao, Y., Wang, X., Sun, T., Sweeney, C.J., Lee, G.-S.M., Chen, S., et al. (2014). Enhancer RNAs participate in androgen receptor-driven looping that selectively enhances gene activation. Proceedings of the National Academy of Sciences *111*, 7319–7324.

Huang, D.W., Sherman, B.T., and Lempicki, R.A. (2009). Systematic and integrative analysis of large gene lists using DAVID bioinformatics resources. Nat Protoc *4*, 44–57.

Huppertz, I., Attig, J., D'Ambrogio, A., Easton, L.E., Sibley, C.R., Sugimoto, Y., Tajnik, M., König, J., and Ule, J. (2014). iCLIP: protein-RNA interactions at nucleotide resolution. Methods *65*, 274–287.

Jin, Q., Yu, L.-R., Wang, L., Zhang, Z., Kasper, L.H., Lee, J.-E., Wang, C., Brindle, P.K., Dent, S.Y.R., and Ge, K. (2011). Distinct roles of GCN5/PCAF-mediated H3K9ac and CBP/p300-mediated H3K18/27ac in nuclear receptor transactivation. Embo J *30*, 249–262.

Kagey, M.H., Newman, J.J., Bilodeau, S., Zhan, Y., Orlando, D.A., van Berkum, N.L., Ebmeier, C.C., Goossens, J., Rahl, P.B., Levine, S.S., et al. (2010). Mediator and cohesin connect gene expression and chromatin architecture. Nature *467*, 430–435.

Kaikkonen, M.U., Spann, N.J., Heinz, S., Romanoski, C.E., Allison, K.A., Stender, J.D., Chun, H.B., Tough, D.F., Prinjha, R.K., Benner, C., et al. (2013). Remodeling of the enhancer landscape during macrophage activation is coupled to enhancer transcription. Mol Cell *51*, 310–325.

Kaneko, S., Bonasio, R., Saldaña-Meyer, R., Yoshida, T., Son, J., Nishino, K., Umezawa, A., and Reinberg, D. (2014a). Interactions between JARID2 and Noncoding RNAs Regulate PRC2 Recruitment to Chromatin. Mol Cell *53*, 290–300.

Kaneko, S., Son, J., Bonasio, R., Shen, S.S., and Reinberg, D. (2014b). Nascent RNA interaction keeps PRC2 activity poised and in check. Genes Dev *28*, 1983–1988.

Kaneko, S., Son, J., Shen, S.S., Reinberg, D., and Bonasio, R. (2013). PRC2 binds active promoters and contacts nascent RNAs in embryonic stem cells. Nat Struct Biol *20*, 1258–1264.

Kasper, L.H., Lerach, S., Wang, J., Wu, S., Jeevan, T., and Brindle, P.K. (2010). CBP/p300 double null cells reveal effect of coactivator level and diversity on CREB transactivation. Embo J *29*, 3660–3672.

Kasper, L.H., Qu, C., Obenauer, J.C., McGoldrick, D.J., and Brindle, P.K. (2014). Genome-wide and single-cell analyses reveal a context dependent relationship between CBP recruitment and gene expression. Nar *42*, 11363–11382.

Kim, T.-K., and Shiekhattar, R. (2015). Architectural and Functional Commonalities between Enhancers and Promoters. Cell *162*, 948–959.

Kim, T.-K., Hemberg, M., Gray, J.M., Costa, A.M., Bear, D.M., Wu, J., Harmin, D.A., Laptewicz, M., Barbara-Haley, K., Kuersten, S., et al. (2010). Widespread transcription at neuronal activity-regulated enhancers. Nature *465*, 182–187.

Lai, F., Orom, U.A., Cesaroni, M., Beringer, M., Taatjes, D.J., Blobel, G.A., and Shiekhattar, R. (2013). Activating RNAs associate with Mediator to enhance chromatin architecture and transcription. Nature.

Lam, M.T.Y., Cho, H., Lesch, H.P., Gosselin, D., Heinz, S., Tanaka-Oishi, Y., Benner, C., Kaikkonen, M.U., Kim, A.S., Kosaka, M., et al. (2013). Rev-Erbs repress macrophage gene expression by inhibiting enhancer-directed transcription. Nature.

Lam, M.T.Y., Li, W., Rosenfeld, M.G., and Glass, C.K. (2014). Enhancer RNAs and regulated

transcriptional programs. Trends Biochem Sci.

Langmead, B., Trapnell, C., Pop, M., and Salzberg, S.L. (2009). Ultrafast and memory-efficient alignment of short DNA sequences to the human genome. Genome Biol *10*, R25.

Li, H., Handsaker, B., Wysoker, A., Fennell, T., Ruan, J., Homer, N., Marth, G., Abecasis, G., Durbin, R., 1000 Genome Project Data Processing Subgroup (2009). The Sequence Alignment/Map format and SAMtools. Bioinformatics *25*, 2078–2079.

Li, W., Notani, D., Ma, Q., Tanasa, B., Nunez, E., Chen, A.Y., Merkurjev, D., Zhang, J., Ohgi, K., Song, X., et al. (2013). Functional roles of enhancer RNAs for oestrogen-dependent transcriptional activation. Nature.

Lienert, F., Mohn, F., Tiwari, V.K., Baubec, T., Roloff, T.C., Gaidatzis, D., Stadler, M.B., and Schübeler, D. (2011). Genomic prevalence of heterochromatic H3K9me2 and transcription do not discriminate pluripotent from terminally differentiated cells. PLoS Genet *7*, e1002090.

Liu, X., Wang, L., Zhao, K., Thompson, P.R., Hwang, Y., Marmorstein, R., and Cole, P.A. (2008). The structural basis of protein acetylation by the p300/CBP transcriptional coactivator. Nature *451*, 846–850.

Lowary, P.T., and Widom, J. (1998). New DNA sequence rules for high affinity binding to histone octamer and sequence-directed nucleosome positioning. J Mol Biol *276*, 19–42.

Luger, K., Rechsteiner, T.J., and Richmond, T.J. (1999). Expression and purification of recombinant histones and nucleosome reconstitution. Methods Mol Biol *119*, 1–16.

Mansour, M.R., Abraham, B.J., Anders, L., Berezovskaya, A., Gutierrez, A., Durbin, A.D., Etchin, J., Lawton, L., Sallan, S.E., Silverman, L.B., et al. (2014). Oncogene regulation. An oncogenic super-enhancer formed through somatic mutation of a noncoding intergenic element. Science *346*, 1373–1377.

Martin, M. (2011). Cutadapt removes adapter sequences from high-throughput sequencing reads. EMBnet J. *17*, 10.

Matys, V., Kel-Margoulis, O.V., Fricke, E., Liebich, I., Land, S., Barre-Dirrie, A., Reuter, I., Chekmenev, D., Krull, M., Hornischer, K., et al. (2006). TRANSFAC and its module TRANSCompel: transcriptional gene regulation in eukaryotes. Nar *34*, D108–D110.

May, D., Blow, M.J., Kaplan, T., McCulley, D.J., Jensen, B.C., Akiyama, J.A., Holt, A., Plajzer-Frick, I., Shoukry, M., Wright, C., et al. (2012). Large-scale discovery of enhancers from human heart tissue. Nat Genet *44*, 89–93.

Melo, C.A., Drost, J., Wijchers, P.J., van de Werken, H., de Wit, E., Oude Vrielink, J.A.F., Elkon, R., Melo, S.A., Léveillé, N., Kalluri, R., et al. (2013). eRNAs are required for p53-dependent enhancer activity and gene transcription. Mol Cell *49*, 524–535.

Meng, F.-L., Du, Z., Federation, A., Hu, J., Wang, Q., Kieffer-Kwon, K.-R., Meyers, R.M., Amor, C., Wasserman, C.R., Neuberg, D., et al. (2014). Convergent transcription at intragenic super-enhancers targets AID-initiated genomic instability. Cell *159*, 1538–1548.

Mousavi, K., Zare, H., Dell'Orso, S., Grontved, L., Gutierrez-Cruz, G., Derfoul, A., Hager, G.L., and Sartorelli, V. (2013). eRNAs Promote Transcription by Establishing Chromatin Accessibility at Defined Genomic Loci. Mol Cell *51*, 606–617.

Perissi, V., Dasen, J.S., Kurokawa, R., Wang, Z., Korzus, E., Rose, D.W., Glass, C.K., and Rosenfeld, M.G. (1999). Factor-specific modulation of CREB-binding protein acetyltransferase activity. Pnas *96*, 3652–3657.

1356 Peterson, C.L. (2008). Salt gradient dialysis reconstitution of nucleosomes. CSH Protoc *2008*,
1357 pdb.prot5113.

1358 Pnueli, L., Rudnizky, S., Yosefzon, Y., and Melamed, P. (2015). RNA transcribed from a distal
1359 enhancer is required for activating the chromatin at the promoter of the gonadotropin α-subunit
1360 gene. Proceedings of the National Academy of Sciences *112*, 4369–4374.

1361 Postepska-Igielska, A., Giwojna, A., Gasri-Plotnitsky, L., Schmitt, N., Dold, A., Ginsberg, D., and
1362 Grummt, I. (2015). LncRNA Khps1 Regulates Expression of the Proto-oncogene SPHK1 via
1363 Triplex-Mediated Changes in Chromatin Structure. Mol Cell *60*, 626–636.

1364 Quinlan, A.R., and Hall, I.M. (2010). BEDTools: a flexible suite of utilities for comparing genomic
1365 features. Bioinformatics *26*, 841–842.

1366 Rada-Iglesias, A., Bajpai, R., Swigut, T., Brugmann, S.A., Flynn, R.A., and Wysocka, J. (2011). A
1367 unique chromatin signature uncovers early developmental enhancers in humans. Nature *470*, 279–
1368 283.

1369 Ryder, S.P., Recht, M.I., and Williamson, J.R. (2008). Quantitative analysis of protein-RNA
1370 interactions by gel mobility shift. Methods Mol Biol *488*, 99–115.

1371 Sammons, M.A., Zhu, J., Drake, A.M., and Berger, S.L. (2015). TP53 engagement with the
1372 genome occurs in distinct local chromatin environments via pioneer factor activity. Genome Res
1373 *25*, 179–188.

1374 Schaukowitch, K., Joo, J.-Y., Liu, X., Watts, J.K., Martinez, C., and Kim, T.-K. (2014). Enhancer
1375 RNA Facilitates NELF Release from Immediate Early Genes. Mol Cell.

1376 Schindelin, J., Arganda-Carreras, I., Frise, E., Kaynig, V., Longair, M., Pietzsch, T., Preibisch, S.,
1377 Rueden, C., Saalfeld, S., Schmid, B., et al. (2012). Fiji: an open-source platform for biological-
1378 image analysis. Nat Methods *9*, 676–682.

1379 Schröder, S., Herker, E., Itzen, F., He, D., Thomas, S., Gilchrist, D.A., Kaehlcke, K., Cho, S.,
1380 Pollard, K.S., Capra, J.A., et al. (2013). Acetylation of RNA polymerase II regulates growth-factor-
1381 induced gene transcription in mammalian cells. Mol Cell *52*, 314–324.

1382 Shah, P.P., Donahue, G., Otte, G.L., Capell, B.C., Nelson, D.M., Cao, K., Aggarwala, V.,
1383 Cruickshanks, H.A., Rai, T.S., McBryan, T., et al. (2013). Lamin B1 depletion in senescent cells
1384 triggers large-scale changes in gene expression and the chromatin landscape. Genes Dev *27*,
1385 1787–1799.

1386 Shen, Y., Yue, F., McCleary, D.F., Ye, Z., Edsall, L., Kuan, S., Wagner, U., Dixon, J., Lee, L.,
1387 Lobanenkov, V.V., et al. (2012). A map of the cis-regulatory sequences in the mouse genome.
1388 Nature *488*, 116–120.

1389 Speir, M.L., Zweig, A.S., Rosenbloom, K.R., Raney, B.J., Paten, B., Nejad, P., Lee, B.T., Learned,
1390 K., Karolchik, D., Hinrichs, A.S., et al. (2016). The UCSC Genome Browser database: 2016
1391 update. Nar *44*, D717–D725.

1392 Stasevich, T.J., Hayashi-Takanaka, Y., Sato, Y., Maehara, K., Ohkawa, Y., Sakata-Sogawa, K.,
1393 Tokunaga, M., Nagase, T., Nozaki, N., McNally, J.G., et al. (2014). Regulation of RNA polymerase
1394 II activation by histone acetylation in single living cells. Nature.

1395 Sun, J., Pan, H., Lei, C., Yuan, B., Nair, S.J., April, C., Parameswaran, B., Klotzle, B., Fan, J.-B.,
1396 Ruan, J., et al. (2011). Genetic and genomic analyses of RNA polymerase II-pausing factor in
1397 regulation of mammalian transcription and cell growth. Journal of Biological Chemistry *286*,
1398 36248–36257.

1399 Tanaka, Y., Tawaramoto-Sasanuma, M., Kawaguchi, S., Ohta, T., Yoda, K., Kurumizaka, H., and
1400 Yokoyama, S. (2004). Expression and purification of recombinant human histones. Methods *33*, 3–
1401 11.

1402 Team, R.C. (2015a). R: A language and environment for statistical computing.

1403 Team, R. (2015b). RStudio Team (2015). RStudio: Integrated Development for R.

1404 Thompson, P.R., Kurooka, H., Nakatani, Y., and Cole, P.A. (2001). Transcriptional coactivator
1405 protein p300. Kinetic characterization of its histone acetyltransferase activity. J Biol Chem *276*,
1406 33721–33729.

1407 Thompson, P.R., Wang, D., Wang, L., Fulco, M., Pediconi, N., Zhang, D., An, W., Ge, Q., Roeder,
1408 R.G., Wong, J., et al. (2004). Regulation of the p300 HAT domain via a novel activation loop. Nat
1409 Struct Biol *11*, 308–315.

1410 Tie, F., Banerjee, R., Stratton, C.A., Prasad-Sinha, J., Stepanik, V., Zlobin, A., Diaz, M.O.,
1411 Scacheri, P.C., and Harte, P.J. (2009). CBP-mediated acetylation of histone H3 lysine 27
1412 antagonizes Drosophila Polycomb silencing. Development *136*, 3131–3141.

1413 Wang, D., Garcia-Bassets, I., Benner, C., Li, W., Su, X., Zhou, Y., Qiu, J., Liu, W., Kaikkonen,
1414 M.U., Ohgi, K.A., et al. (2011). Reprogramming transcription by distinct classes of enhancers
1415 functionally defined by eRNA. Nature *474*, 390–394.

1416 Wang, F., Marshall, C.B., and Ikura, M. (2013). Transcriptional/epigenetic regulator CBP/p300 in
1417 tumorigenesis: structural and functional versatility in target recognition. Cell Mol Life Sci *70*, 3989–
1418 4008.

1419 Wang, L., and Brown, S.J. (2006). BindN: a web-based tool for efficient prediction of DNA and
1420 RNA binding sites in amino acid sequences. Nar *34*, W243–W248.

1421 Wang, L., Tang, Y., Cole, P.A., and Marmorstein, R. (2008a). Structure and chemistry of the
1422 p300/CBP and Rtt109 histone acetyltransferases: implications for histone acetyltransferase
1423 evolution and function. Curr Opin Struct Biol *18*, 741–747.

1424 Wang, Z., Zang, C., Rosenfeld, J.A., Schones, D.E., Barski, A., Cuddapah, S., Cui, K., Roh, T.-Y.,
1425 Peng, W., Zhang, M.Q., et al. (2008b). Combinatorial patterns of histone acetylations and
1426 methylations in the human genome. Nat Genet *40*, 897–903.

1427 Wongtrakoongate, P., Riddick, G., Fucharoen, S., and Felsenfeld, G. (2015). Association of the
1428 Long Non-coding RNA Steroid Receptor RNA Activator (SRA) with TrxG and PRC2 Complexes.
1429 PLoS Genet *11*, e1005615.

1430 Yang, Y.W., Flynn, R.A., Chen, Y., Qu, K., Wan, B., Wang, K.C., Lei, M., and Chang, H.Y. (2014).
1431 Essential role of lncRNA binding for WDR5 maintenance of active chromatin and embryonic stem
1432 cell pluripotency. Elife *3*, e02046.

1433 Yuan, H., Rossetto, D., Mellert, H., Dang, W., Srinivasan, M., Johnson, J., Hodawadekar, S., Ding,
1434 E.C., Speicher, K., Abshiru, N., et al. (2012). MYST protein acetyltransferase activity requires
1435 active site lysine autoacetylation. Embo J *31*, 58–70.

1436 Yuan, L.W., and Giordano, A. (2002). Acetyltransferase machinery conserved in p300/CBP-family
1437 proteins. Oncogene *21*, 2253–2260.

1438 Zhang, Y., Liu, T., Meyer, C.A., Eeckhoute, J., Johnson, D.S., Bernstein, B.E., Nusbaum, C.,
1439 Myers, R.M., Brown, M., Li, W., et al. (2008). Model-based analysis of ChIP-Seq (MACS). Genome
1440 Biol *9*, R137.

1441 Ørom, U.A., Derrien, T., Beringer, M., Gumireddy, K., Gardini, A., Bussotti, G., Lai, F., Zytnicki, M.,
1442 Notredame, C., Huang, Q., et al. (2010). Long noncoding RNAs with enhancer-like function in
1443 human cells. Cell *143*, 46–58.

1444

Figure 1

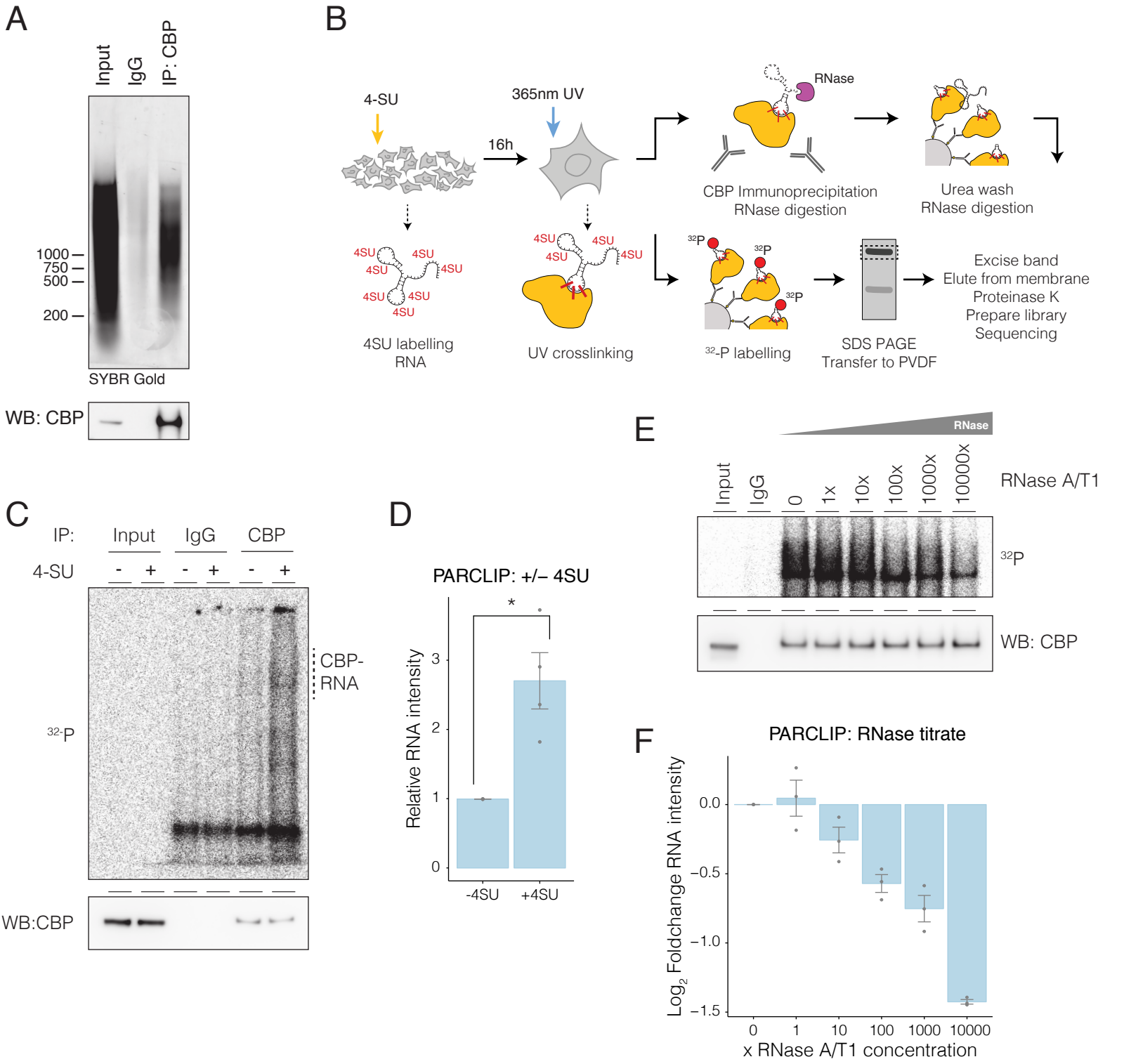

Figure 2

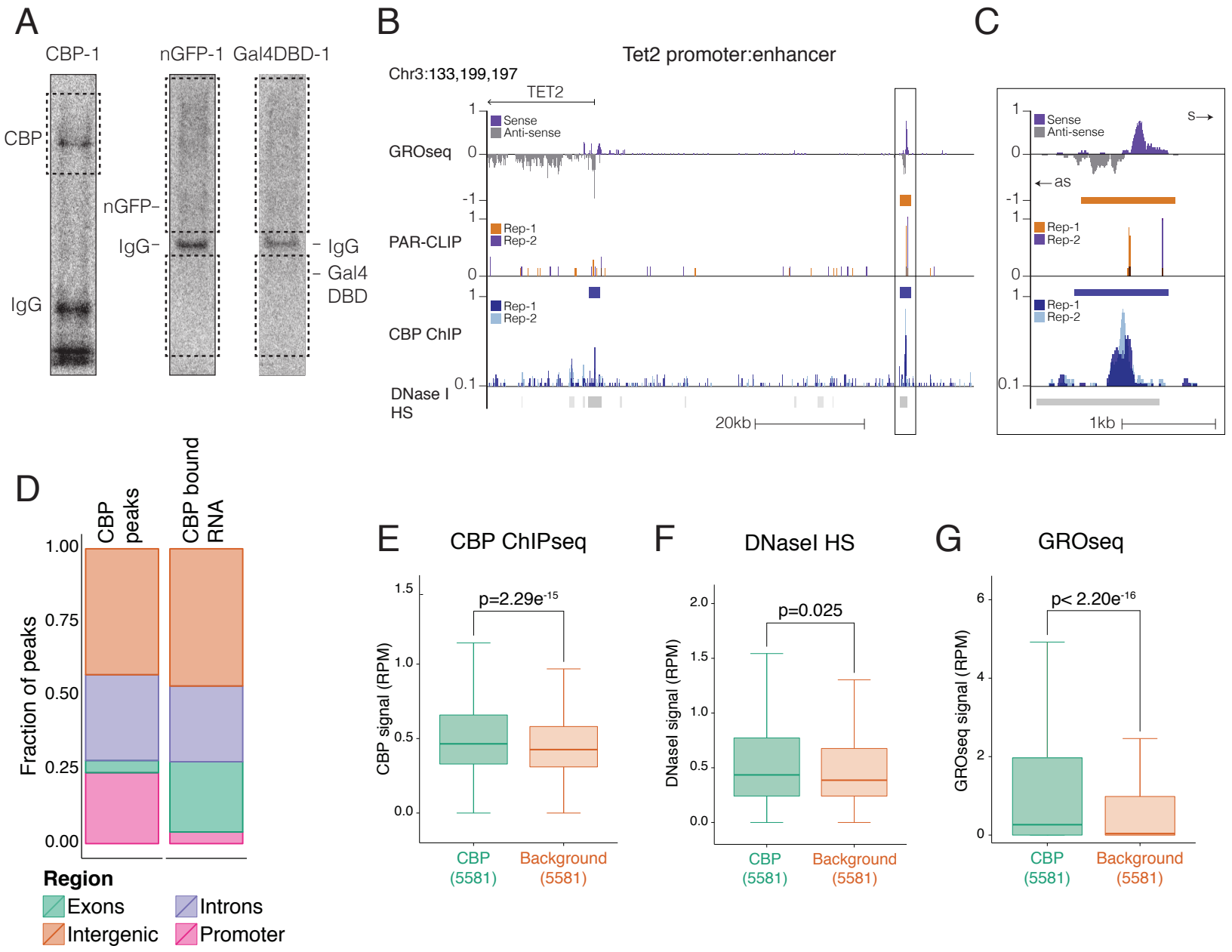

Figure 3

Click here to download Figure Bose.Berger.Figure3.pdf

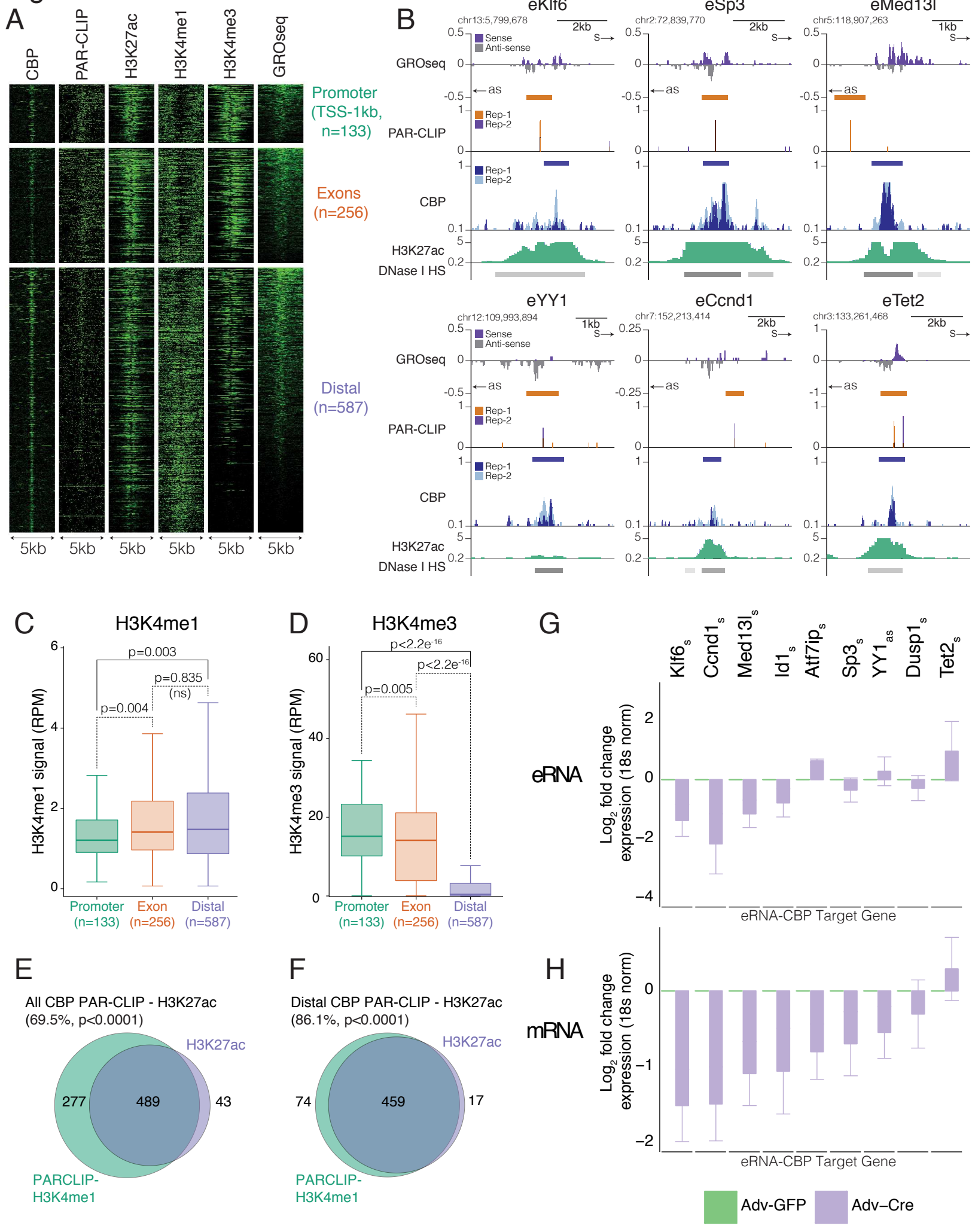

Figure 4

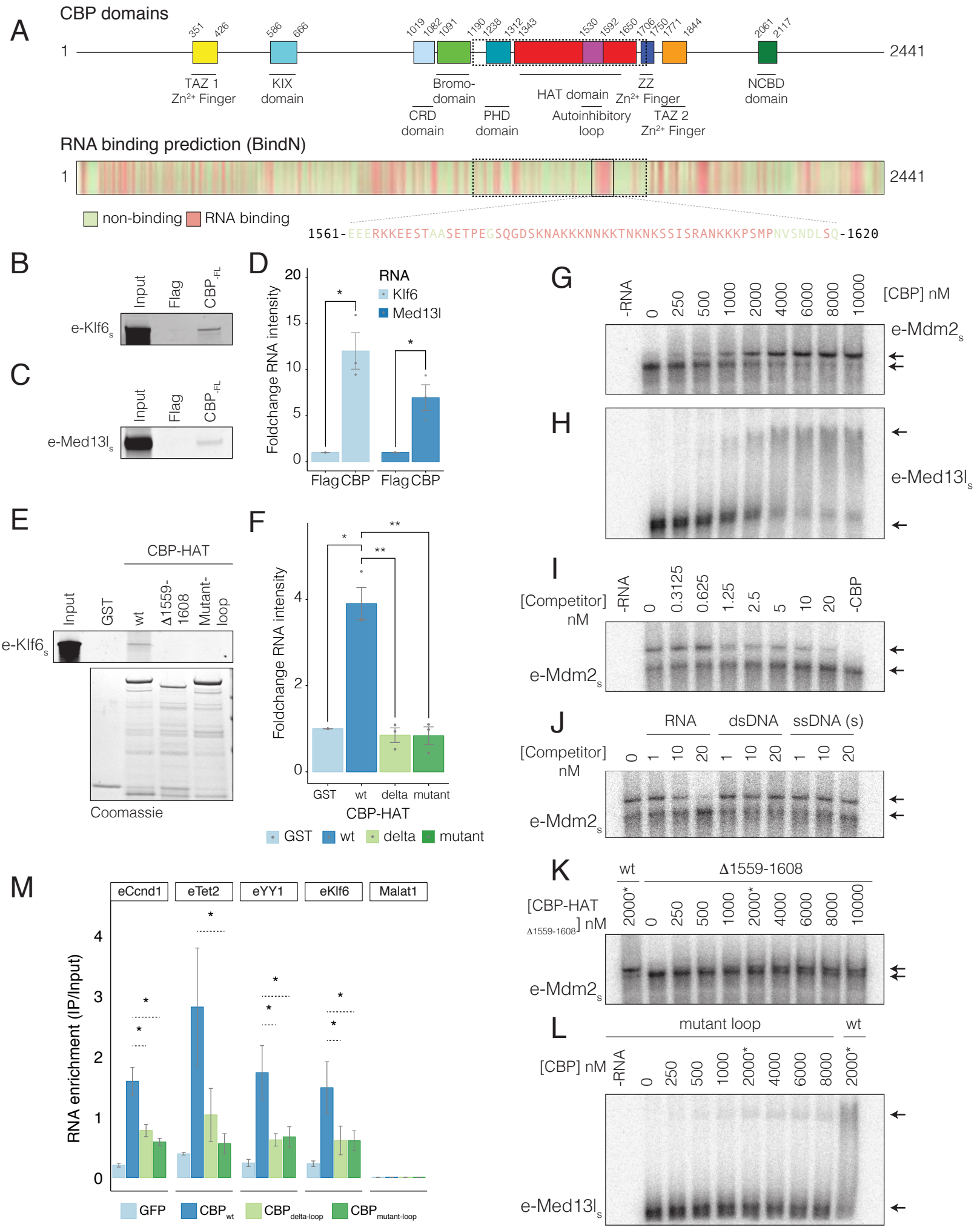

Figure 5

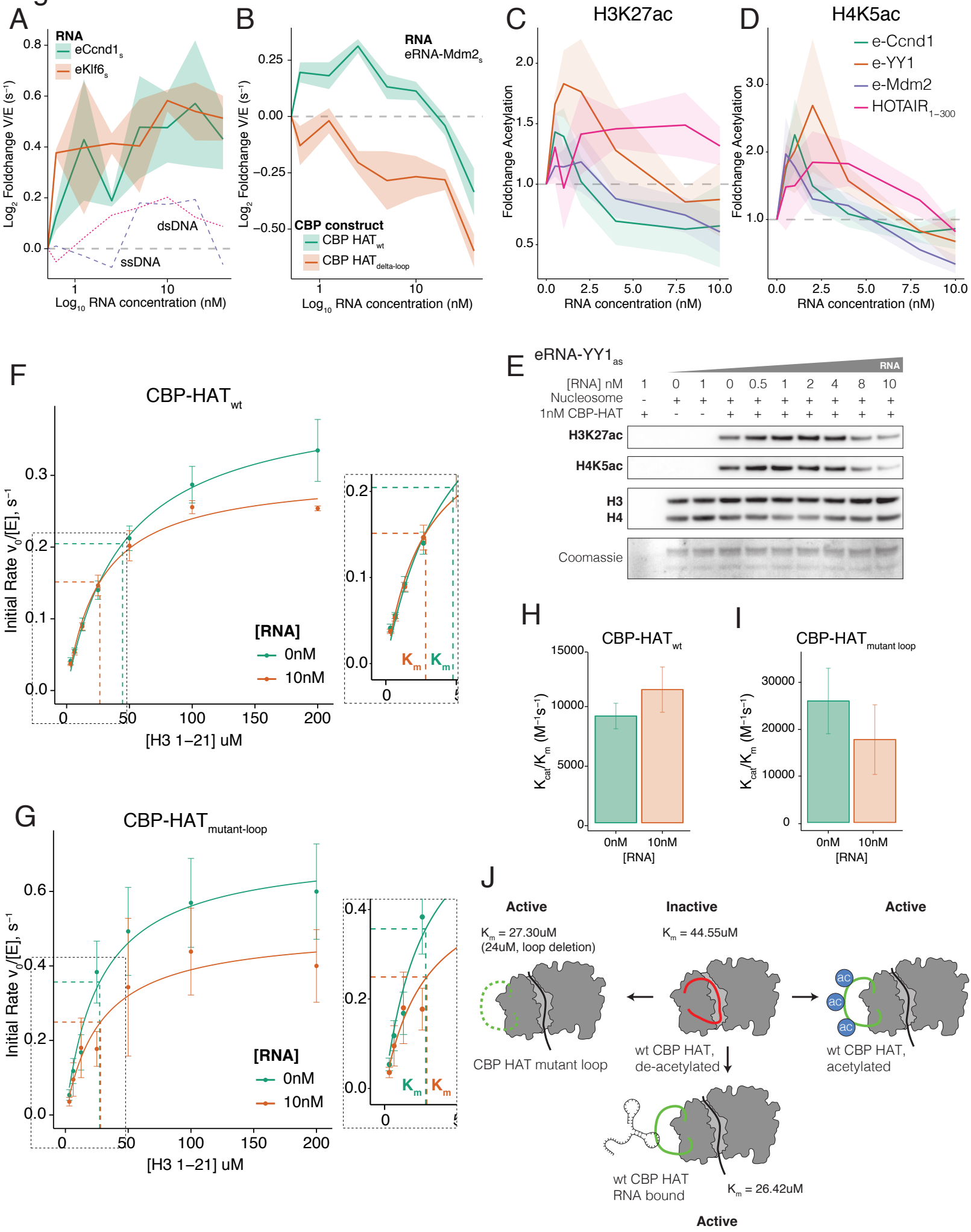

Figure 6

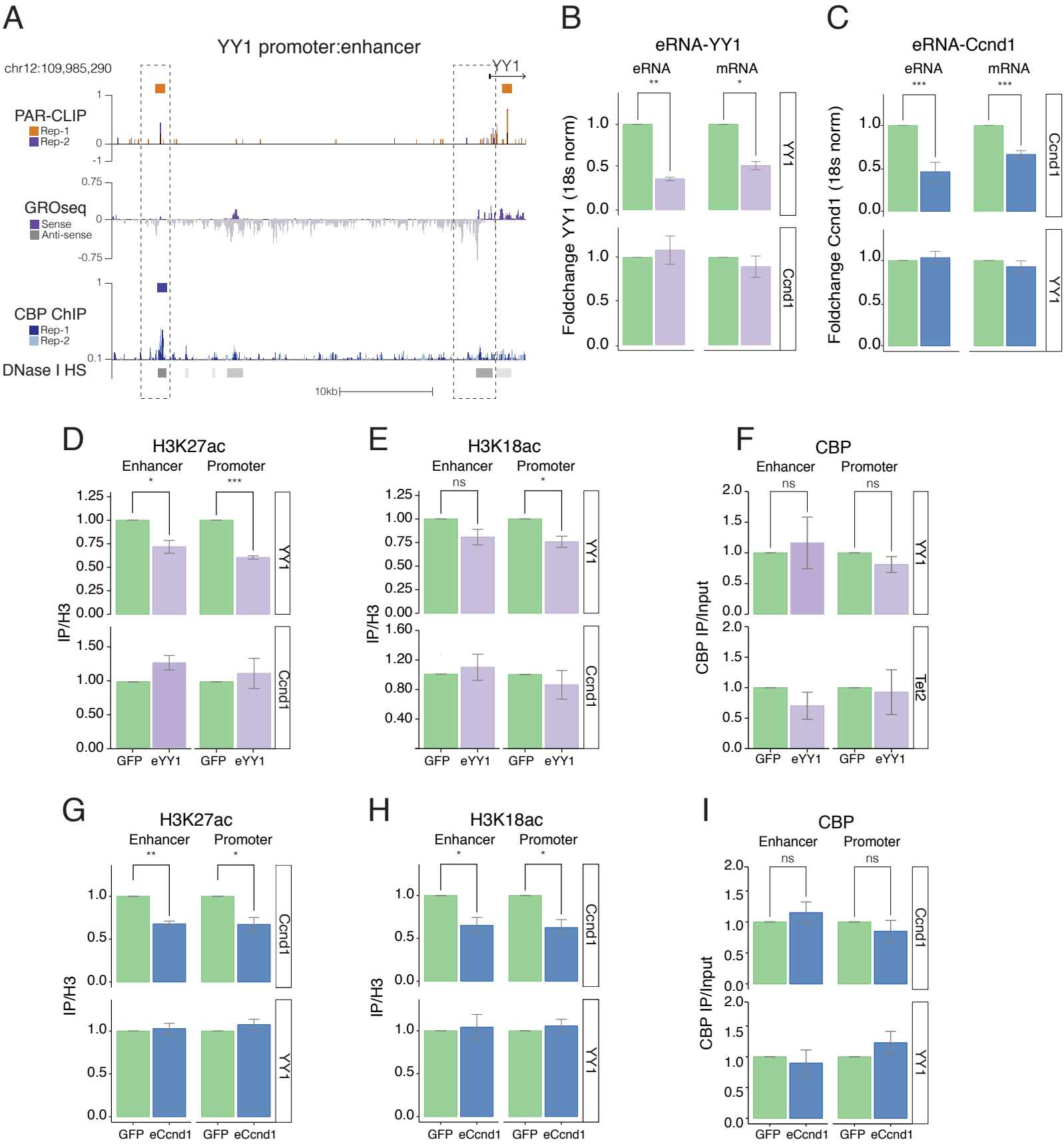

Figure 7

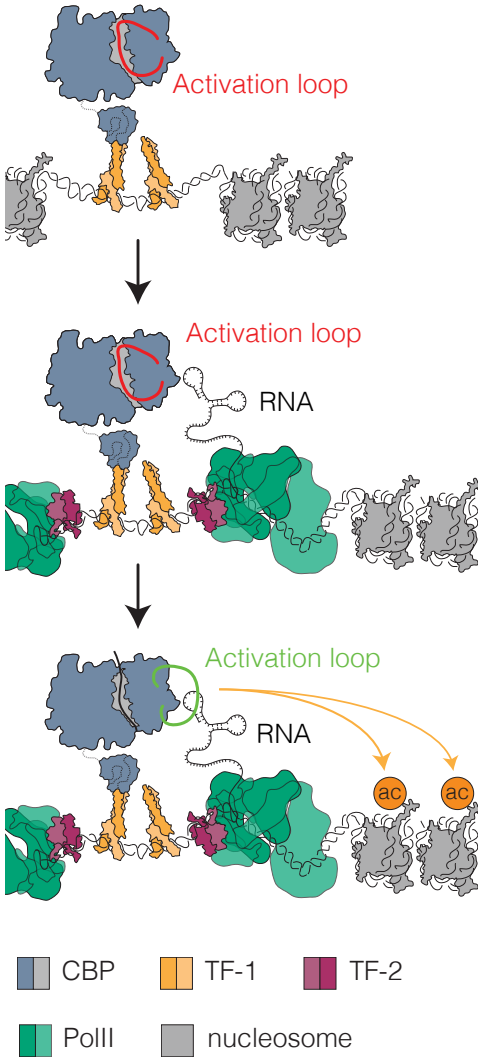

Inactive enhancers
No eRNAs
Activation loop blocks
active site of CBP
Low HAT activity
Low H3K27ac

Activation
PolII recruitment by TFs
eRNA transcription

Active enhancers
eRNA binds to CBP
activation loop
Activation loop displaced
from active site
High HAT activity
High H3K27ac

Supplementary information

Figure S1, related to Figure 1

A) Whole western blot view of Figure 1A

B) Whole autoradiography and western blot view of Figure 1C. CBP PAR-CLIP signal required 4-SU.

C) Western blot for CBP. Input was not ^{32}-P labeled.

D-E) Example replicates of Figure 1C quantified in Figure 1D, CBP PAR-CLIP required 4-SU: Top, Autoradiography; Bottom, western blot for CBP on PAR-CLIP membrane. Input was not ^{32}-P labeled, but resolved and transferred to the same membrane.

F-G) Whole autoradiography (F) and western blot (G) view of Figure 1E, CBP PAR-CLIP signal was sensitive to increasing RNAse concentrations. 1x RNAse cocktail contained: RNAse A (0.01mU/ul) + RNase T1 (0.4mU/ul).

H) Example replicate autoradiography of Figure 1E, quantified in Figure 1F.

Figure S2, related to Figure 2

A) Autoradiography of 2nd biological replicate of CBP PAR-CLIP and nls-GFP (nGFP) and yeast Gal4 DNA binding domain (Gal4-DBD) background control membranes. Dashed box shows regions of membrane excised for library preparation.

B) Correlation of PAR-CLIP reads from individual replicates 1 and 2 over CBP enriched RNAs called from replicate 1 (5926) and 2 (5322). Correlation of reads from replicate 1 and 2 over common peaks that were called independently in both replicates (3229) are highlighted in red.

C) Distribution of sizes of CBP-RNA regions following assignment of statistically enriched RNAs with PARalyzer v1.1.

D-G) Intersection of CBP-RNAs with background control RNAs: D) Gal4-DBD control intersecting nGFP control; E) CBP enriched RNA intersecting Gal4-DBD control; F) CBP enriched RNA intersecting nGFP control; G) CBP enriched RNA intersecting Gal4-DBD and nGFP control RNAs.

H) Immunoprecipitation of CBP under Native RNA-IP conditions +/- treatment with 1mg/ml RNase A; WB for Mediator (Med-1 subunit) or NELF (NELF-e subunit).

I) Immunoprecipitation of CBP under PAR-CLIP conditions; WB for Mediator (Med-1 subunit) or NELF (NELF-e subunit).

J) Comparison of Mediator (GSM560353 (Kagey et al., 2010), left panel) and NELFb (GSE24113 (Sun et al., 2011), right panel) read density over CBP-RNAs and enriched control RNAs. CBP peaks were randomly downsampled to match the size of the background dataset (5581).

K-L) Enrichment of reads at CBP-RNAs sorted by genome regions from Figure 2D; L) CBP-RNA (PAR-CLIP) signal; M) Nascent RNA transcription (GROseq) signal (Promoter = 1kb upstream of TSS).

M) Read density of total RNAseq datasets (GSM687308, right panel; GSM1100747, left panel) at CBP-RNAs.

N-O) Comparison of nascent transcription (GROseq) and total RNAseq at CBP-RNAs; N) Enrichment of total RNAseq reads at CBP-RNAs. CBP-RNAs were grouped into deciles based on GROseq signal (10^{th} decile = most enriched for GROseq reads). Boxplot shows total RNAseq reads (GSM1100747); O) Enrichment of GROseq signal at CBP-RNAs. CBP-RNAs were grouped into deciles based total RNAseq signal (10^{th} decile = most enriched for total RNAseq reads). Boxplot shows total GROseq reads.

P) Comparison of GROseq and total RNAseq (GSM1100747) enrichment at CBP-RNAs sorted by genome regions from Figure 2D. *P*-values from Mann-Whitney U-test.

Q) Spearman correlation co-efficient between PAR-CLIP and CBP ChIPseq reads over 1kb intersecting bound RNA regions at increasing peak-to-peak distances. Plot shows correlation for CBP bound RNAs (purple), Gal4-DBD (orange) and nGFP (green) background control bound RNAs. Grey dashed line highlights a 3.5kb peak-peak distance.

Figure S3, related to Figure 3

A-C) Comparison of read density (RPM) over enriched RNA regions <3.5kb from nearest CBP peak and >3.5kb from nearest CBP peak; A) CBP PAR-CLIP; B) CBP ChIPseq; C) GROseq. *P*-values from Mann-Whitney U-test.

D) Histogram showing distance from RNA bound CBP peaks to nearest TSS. Peaks were divided into Promoter (TSS-1kb), Exon and Distal (intronic/intergenic) sub groups.

E) Comparison of CBP signal at RNA-bound CBP peaks (<3.5kb) in Promoter, Exon and Distal groups. CBP peaks were sorted into deciles based on PAR-CLIP enrichment. Boxplots show enrichment for CBP ChIPseq reads at each decile (10^{th} decile = most enriched for total PAR-CLIP reads).

F) Comparison of PAR-CLIP signal at RNA-bound CBP peaks (<3.5kb) in Promoter, Exon and Distal groups. CBP peaks were sorted into deciles based on CBP enrichment. Boxplots show enrichment for PAR-CLIP reads at the top five deciles for CBP signal (10^{th} decile = most enriched for total CBP ChIPseq reads).

G) Comparison of PAR-CLIP signal at RNA-bound CBP peaks (<3.5kb) in Promoter, Exon and Distal groups. CBP peaks were sorted into deciles based on GROseq enrichment. Boxplots show enrichment for PAR-CLIP reads at the top five deciles for GROseq signal (10^{th} decile = most enriched for total GROseq reads).

H-M) Comparison of RNA-CBP peaks in Promoter, Exon and Distal subgroups. Profiles show 50bp bins over 5kb windows centered on the CBP peak and were normalized by number of peaks in each genome region subgroup; Promoter (green), Exon (orange), Distal (purple). Grey boxes show the 1kb window used for quantification in box-plots; H) Read density profiles of CBP reads; I) Quantification of CBP read density; J) Read density profiles of GROseq reads; K) Quantification of GROseq read density; L) Read density profiles of PAR-CLIP reads; M) Quantification of PAR-CLIP read density. All reads were normalized per million mapped reads (RPM). *P*-values from Mann-Whitney U-test.

N) Boxplot shows H3K27ac reads over RNA bound CBP peaks (green) or non-RNA bound CBP peaks (orange). *P*-values from Mann-Whitney U-test. non-RNA bound CBP peaks were randomly downsampled to match CBP-eRNA peaks (976).

O) GROseq read density profiles (RPM) comparing RNA bound CBP peaks (green) or non-RNA bound CBP peaks (orange). non-RNA bound CBP peaks were randomly downsampled to match CBP-eRNA peaks (976).

P-R) Venn diagrams showing overlap between: P) RNA bound CBP peaks and H3K4me1; Q) RNA bound CBP peaks and H3K27ac; R) All CBP peaks with H3K4me1 peaks and H3K27ac peaks.

S) GO analysis (DAVID, (Huang et al., 2009)) of nearest genes to PAR-CLIP CBP peaks. (FDR <1, sorted by FDR).

T) Comparison of CBP-eRNA associated genes with genes not associated with CBP-eRNA. Control population was downsized to match the 1146 genes proximal to CBP-eRNA (Gene expression microarray data from GSE54452, (Kasper et al., 2014)).*P*-values from Mann-Whitney U-test.

U) RT-qPCR data showing fold change in CBP mRNA following infection with control adenoviral GFP (Adv-GFP, green) or knockdown with Adenoviral Cre (Adv-Cre, purple). Error bars represent mean +/- s.e.m; n=4; *P*-values from two-tailed Student's t-test.

Figure S4, related to Figure 4

A) RNA binding prediction (BindN, (Wang and Brown, 2006)) for CBP-HAT domain. Predictions for non-binding residues (green) and binding residues (red) are indicated. Residues forming the activation loop and residues 1559-1608 deleted or mutated to prevent RNA binding are highlighted.

B) Purification of flag-tagged recombinant CBP from Sf9 cells (Left panel) and GST tagged CBP-HAT domain from *E.coli* (Right panel). Both gels were stained with Coomassie.

C-D) Replicate gel images of Figure 4B-C; *In vitro* pull down of C) eRNA-Klf6$_s$ and D) eRNA-Med13l$_s$ using flag-tagged CBP. s=sense, as=antisense strand RNA.

E) *In vitro* pull down of eRNA-Klf6 using GST-tagged CBP HAT domain constructs (see also Figure 4C). RNA fraction stained with SYBR gold is shown in top panel; protein fractions stained with coomassie are shown in bottom panel.

F) *In vitro* pull down of diverse RNA sequences using CBP-HAT$_{wt}$. eRNA sequences eRNA-Tet2s, eRNA-Klf4s, eRNA-Klf6s (left); lncRNA sequences HOTAIR1-300, Gas5, Meg3 (middle); exonic RNA sequences (ID-1 (exon1), Bbs2 (exon-1), Klf2 (exon-2) (right). All RNAs were resolved using 6% TBE Urea gels, apart from Meg3 (resolved using denaturing agarose formaldehyde gel) and stained using SYBR Gold.

G) Quantification of RNA-pulldown data in Figure S4F. n=3.

H) Binding curves showing eRNA binding to CBP-HAT$_{wt}$.

I) GST CBP-HAT domain constructs used in EMSAs showing CBP-HAT$_{wt}$, CBP-HAT$_{delta\text{-}loop}$ and CBP-HAT$_{mutant\ loop}$ constructs. Constructs were designed with reference to predicted RNA binding residues (Figure S4A) and residues deleted in available X-ray crystallographic structures of the p300 HAT domain. In the mutant loop sequence, mutated residues are highlighted in lower case.

J) RNA EMSA showing requirement for de-acetylation for RNA binding. GST-CBP-HAT$_{wt}$ was expressed without co-expressing ySir2 and purified (CBP-HAT$_{ac}$). 2nM eRNA-YY1 was titrated with 0-10000nM CBP-HAT$_{ac}$.

K) RNA EMSA using CBP-HAT$_{mutant\text{-}loop}$. eRNA-Ccnd1 was titrated with stated concentrations of CBP-HAT$_{mutant\ loop}$. (*) CBP-HAT$_{wt}$ (2000nM).

L) Western blot for immunoprecipitated GFP-CBP (control for Figure 4M).

M) Additional eRNAs (i-iv) and replicated gel images (v-x): RNA EMSA of eRNA probes using CBP-HAT$_{wt}$ (0-10000nM); i) eRNA-YY1$_s$; ii) eRNA-Klf6$_s$; iii) eRNA-Ccnd1$_s$; iv) Competition binding RNA EMSAs. Binding of 2nM ^{32}-P radiolabelled eRNA-YY1 to CBP-HAT$_{wt}$ (2000nM) was competed with 0-20nM un-labelled eRNA-YY1; v-vi) two replicates of eRNA-Mdm2 with CBP-HAT$_{wt}$ (Figure 4G); vii) eRNA-Med13l titration with CBP-HAT$_{wt}$ (Figure 4H); viii) Binding of 2nM ^{32}-P radiolabelled eRNA-Mdm2 to CBP-HAT$_{wt}$ (2000nM) was competed with 1nM, 10nM and 20nM un-labeled eRNA-Mdm2 (RNA), dsDNA or ssDNA with the same sequence; ix) RNA EMSA using CBP-HAT$_{delta\text{-}loop}$. eRNA-Med13l was titrated with 0-10,000nM CBP-HAT$_{delta\text{-}loop}$. (*) CBP-HAT$_{wt}$ (2000nM); x) RNA EMSA using CBP-HAT$_{mutant\text{-}loop}$. eRNA-YY1 was titrated with 0-8000nM CBP-HAT$_{mutant\ loop}$. (*) CBP-HAT$_{wt}$ (2000nM).

N) Whole gel images of RNA EMSA experiments in main and supplementary Figures. Numbers for the original Figures are indicated. *P*-values from two-tailed Student's t-test: *P< 0.05; **P< 0.01; ***P< 0.001.

Figure S5, related to Figure 5

A) Schematic of filter binding HAT assay.

B) *In vitro* pull-down of RNA sequences using CBP-HAT$_{wt}$. lncRNA HOTAIR$_{1-300}$, exonic RNA (ID-1 (exon1) and lncRNA Meg3. All RNAs were resolved using 6% TBE Urea gels, apart from Meg3 (resolved using denaturing agarose formaldehyde gel) and stained using SYBR Gold (same experiment as Figure S4F).
C) RNA dose curve filter binding assays: RNA dependent stimulation of CBP acetyltransferase activity. 5nM CBP-HAT$_{wt}$ was titrated with 0-40nM RNA (lncRNA HOTAIR$_{1-300}$, exonic RNA (ID-1 (exon1) and lncRNA Meg3). Data shows fold change in rate of Acetyl-CoA incorporation (V_{max})/Concentration enzyme ([E], (s^{-1})) from 0nM RNA. Shaded regions represent mean +/- s.e.m (RNA n=3).
D) Native PAGE showing DNA binding to reconstituted nucleosomes (top panel). Coomassie staining showing individual histones (bottom panel).
E-G) Western blot HAT assay using recombinant nucleosome substrate. 1nM CBP-HAT$_{wt}$ was titrated with 0-10nM E) eRNA-Mdm2$_s$; F) eRNA-Ccnd1$_s$; G) lncRNA HOTAIR$_{1-300}$. The reaction was resolved by SDS-PAGE and probed for H3K27ac, H4K5ac and H3/H4 by western blot. Coomassie staining (bottom panel) shows individual histones.
H) Western blot HAT assay. 1nM CBP-HAT$_{wt}$ was titrated with 0-10nM eRNA-Mdm2 (top), eRNA-PAPPA (middle) (Melo et al., 2013) or long noncoding RNA HOTAIR (bottom) (Kaneko et al., 2013). Reaction was resolved by SDS-PAGE and probed for H3K27ac by western blot. Reactions contained 20uM purified recombinant H3.1 and 200uM Acetyl CoA.
I) Quantification of Western blot HAT assays in Figure 5C and Figure S5B. Densitometry was determined in FIJI. For quantified Western blots, n=4).
J) Western blot HAT assay: human MOF (hMOF). 1nM hMOF HAT domain was titrated with 0-10nM eRNA-Mdm2. Reaction was resolved by SDS-PAGE and probed for H3K27ac by western blot. (hMOF was a kind gift of Ronen Marmorstein). Reactions contained 20uM purified recombinant H4 and 200uM Acetyl CoA.
K) Kinetic parameters derived from steady state HAT assays. All analysis was carried out using nls regression in R.
L) RNA integrity was checked before and after each HAT assay (Example control gel of eRNA-Mdm2 from steady state HAT assays). Control reactions contained 200uM unlabeled Acetyl-CoA; RNA was extracted with Trizol and resolved on a denaturing 6% TBE urea gel stained with SYBR gold.

Figure S6, related to Figure 6
A-C) UCSC genome browser view of GROseq signal (+ strand purple, - strand grey) and CBP-RNAs (orange bars) at enhancer and promoter regions for: A) *YY1*; B) *Ccnd1*; C) *Tet2*.
D) ChIP-qPCR for H3K27ac (left) and H3K18ac (right) at enhancer and promoter regions following knockdown of CBP and p300. *CBP/p300 flox/flox* MEFs were infected with control adenoviral GFP (Adv-GFP, Green) or adenoviral Cre (Adv-Cre, purple/blue/orange). Data shows foldchange in IP/H3. Error bars represent mean +/- s.e.m; n=3.
E) ASO mediated depletion of PAR-CLIP eRNA. RT-qPCR data showing foldchange in expression of eRNA and associated mRNA following transfection of ASO targeting eRNA-YY1$_{antisense}$ (purple), eRNA-Ccnd1$_{sense}$ (blue), eRNA-Tet2$_{sense}$ (orange) or GFP-control (green). Depletion efficiency was determined from expression of eRNA and mRNA at *YY1* (top), *Ccnd1* (middle) or *Tet2* (bottom). Error bars represent mean +/- s.e.m; n=4.
F-G) ChIP-qPCR at enhancer and promoter regions following transfection of ASO targeting eRNA-YY1 (purple) or GFP-control (green) showing foldchange in IP/H3 for: F) H3K27ac and G) H3K18ac at targeted gene and non-targeted control gene Tet2 (control, bottom). Error bars represent mean +/- s.e.m; n=4; *P*-values from two-tailed Student's t-test. (Data is from the same experiment as Figure 6F-H)

H-I) ChIP-qPCR at enhancer and promoter regions following transfection of ASO targeting eRNA-Tet2 (orange) or GFP-control (green) showing foldchange in IP/H3 for: H) H3K27ac and I) H3K18ac at targeted gene *Tet2* and non-targeted control gene *YY1* (bottom). Error bars represent mean +/- s.e.m; n=4; *P*-values from two-tailed Student's t-test.
J) CBP ChIP-qPCR at targeted gene *Tet2* and non-targeted control gene *YY1*. Data shows foldchange in CBP IP/Input. Error bars represent mean +/- s.e.m; n=4; *P*-values from two-tailed Student's t-test: *P< 0.05; **P< 0.01; ***P< 0.001.

Figure S1

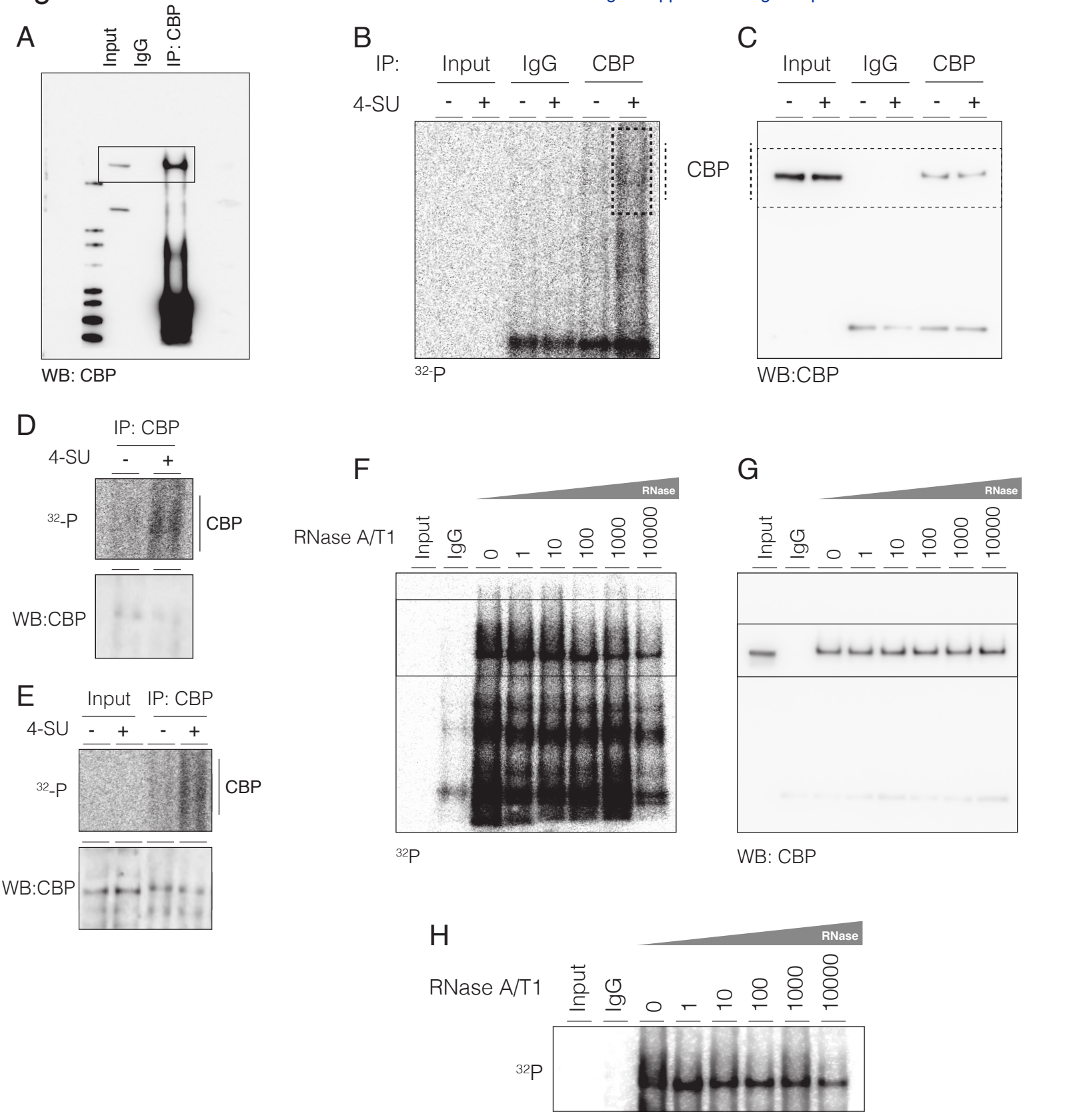

Figure S2

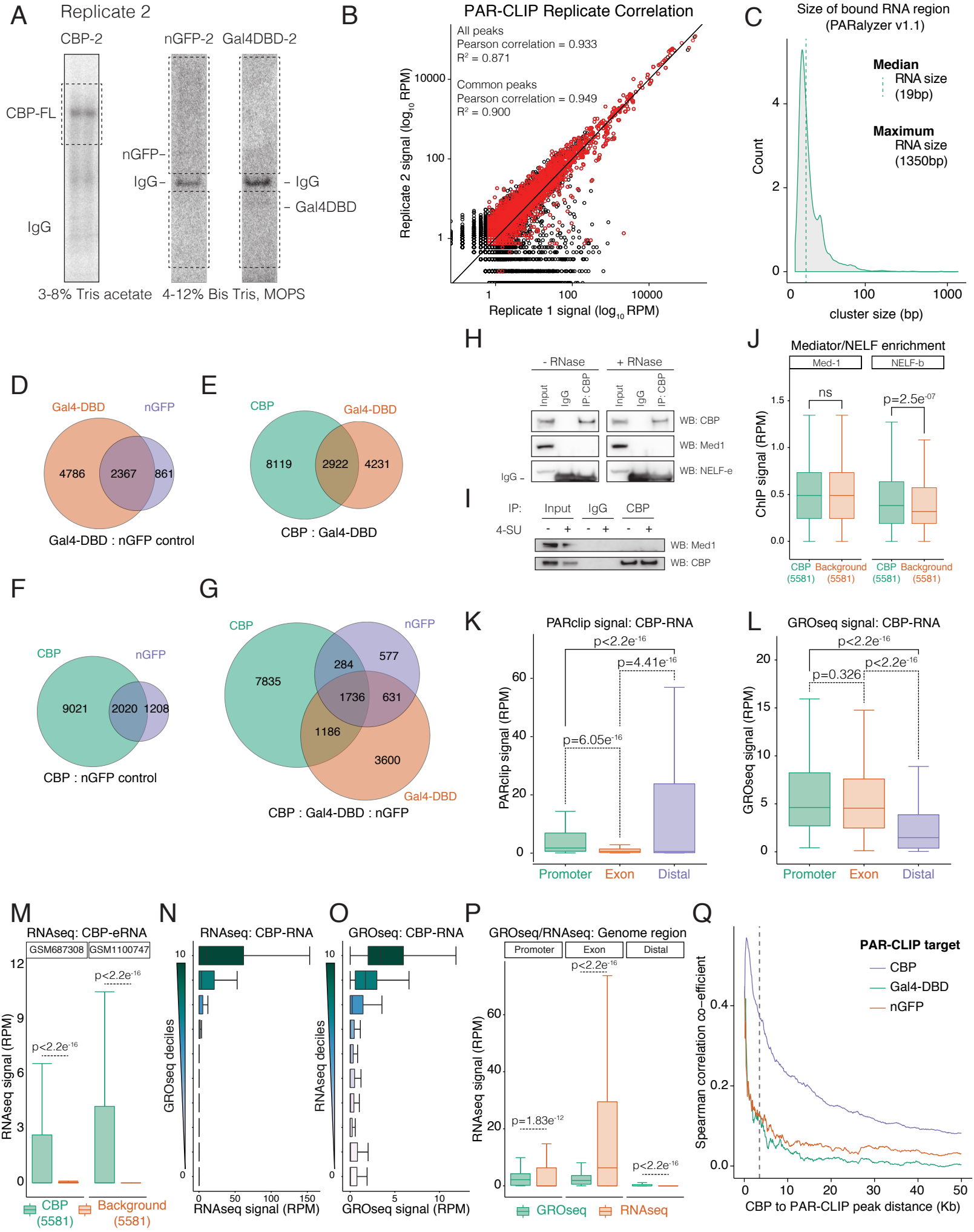

Supplemental Figure-3

Figure S3

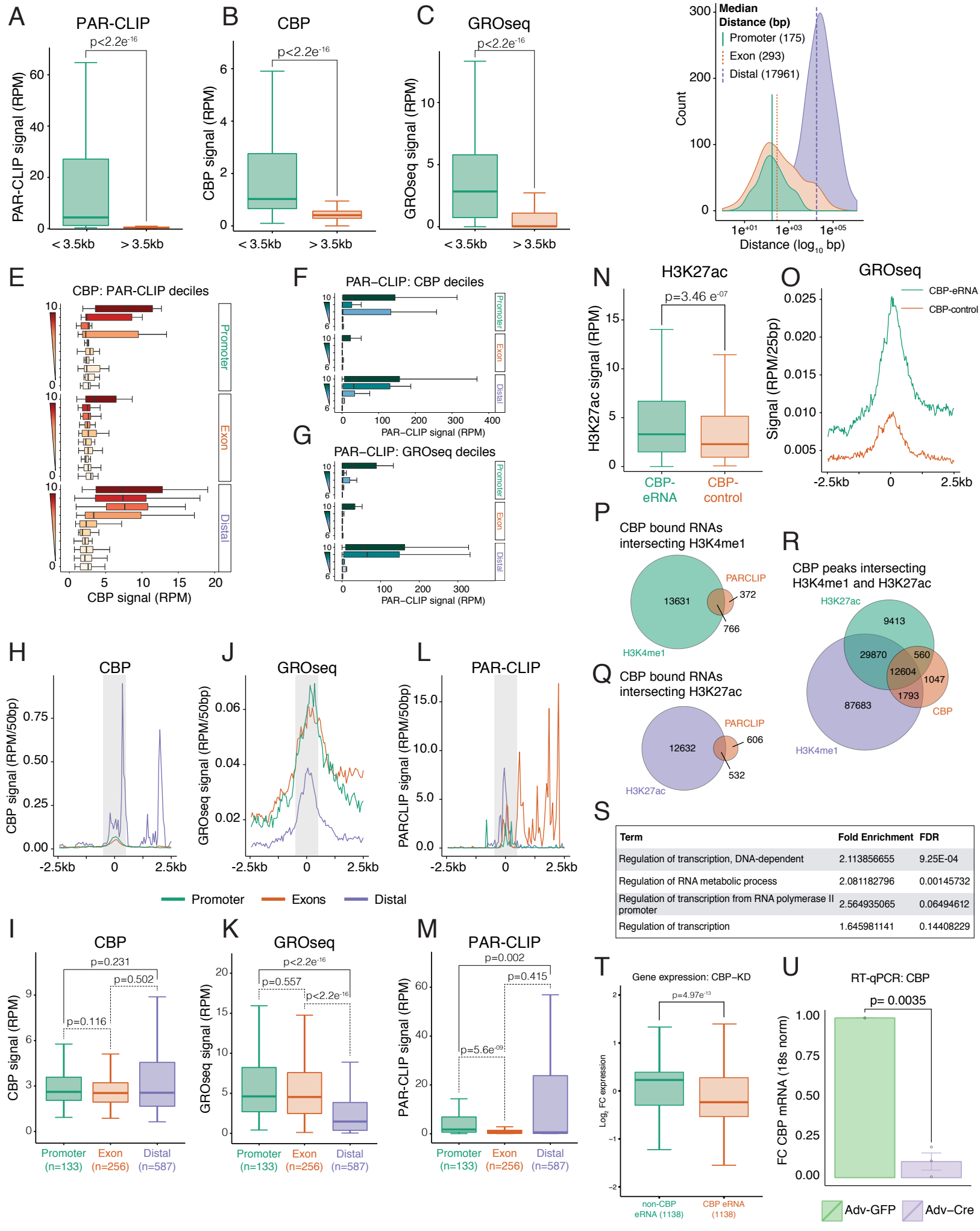

Figure S4

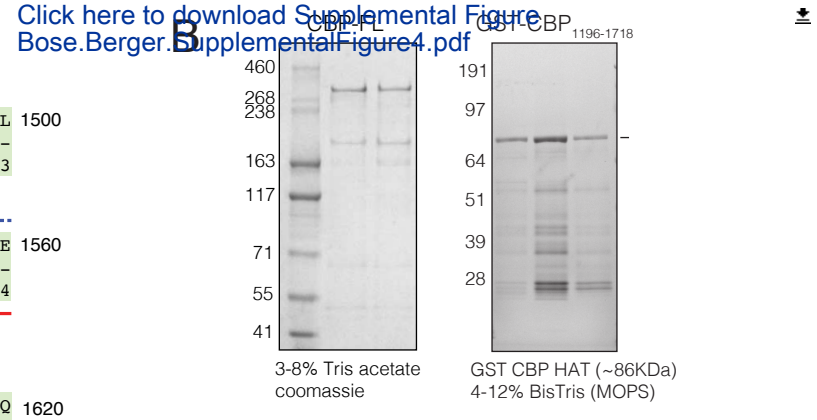

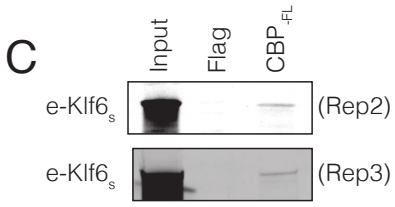

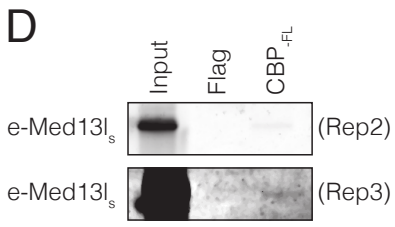

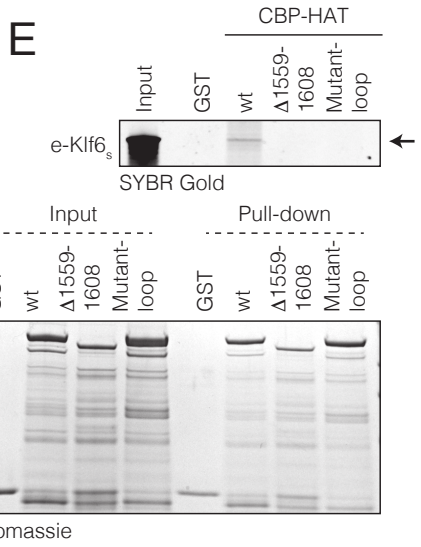

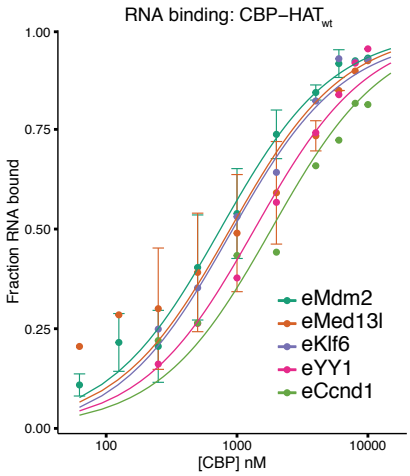

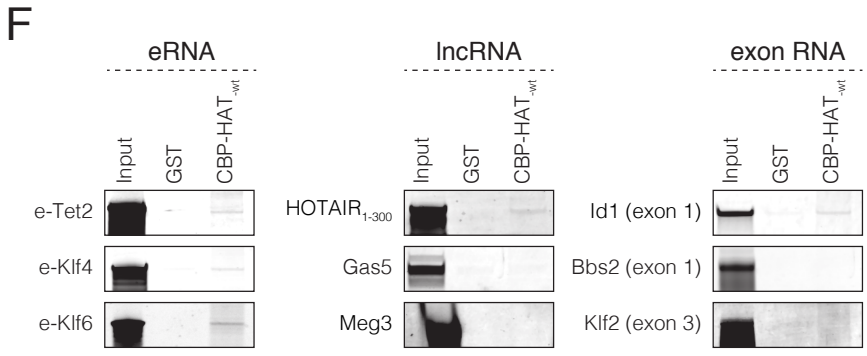

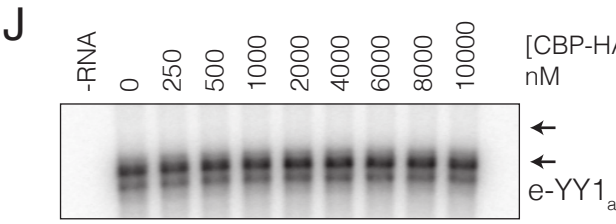

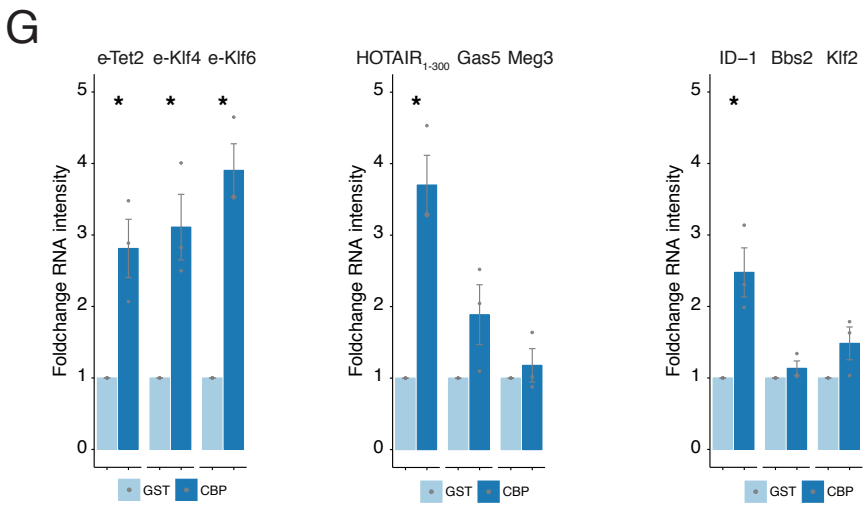

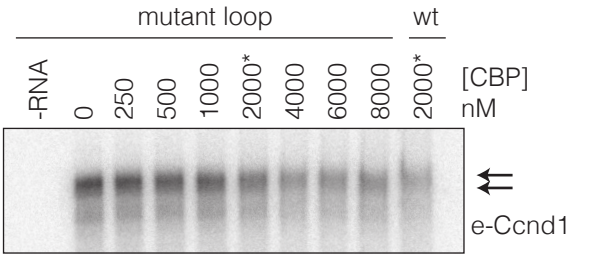

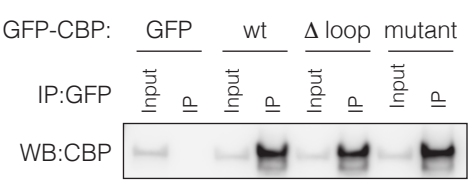

Figure S5

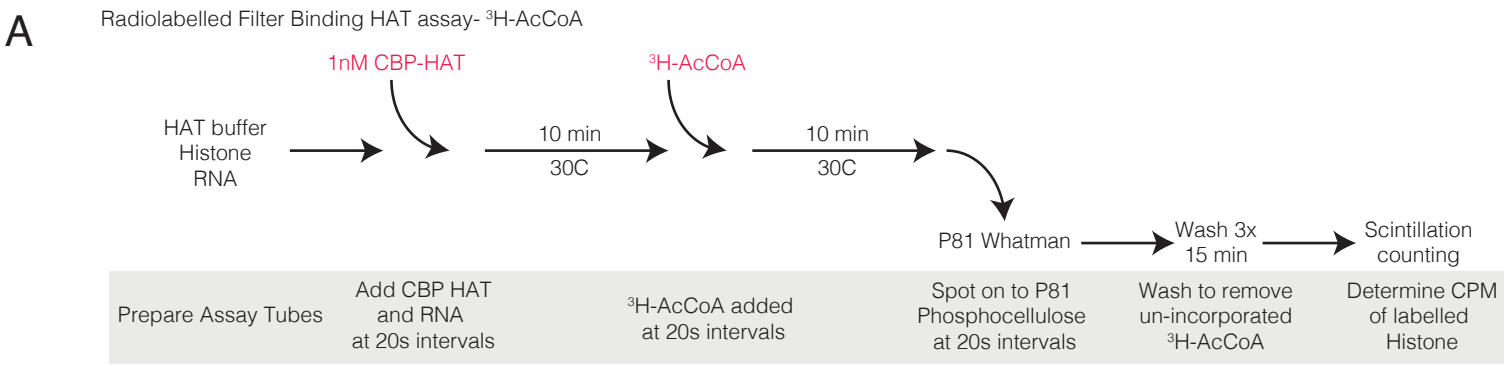

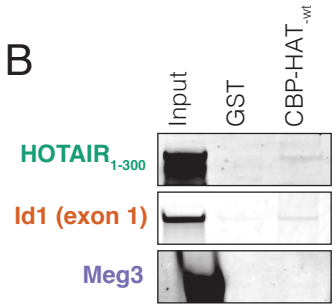

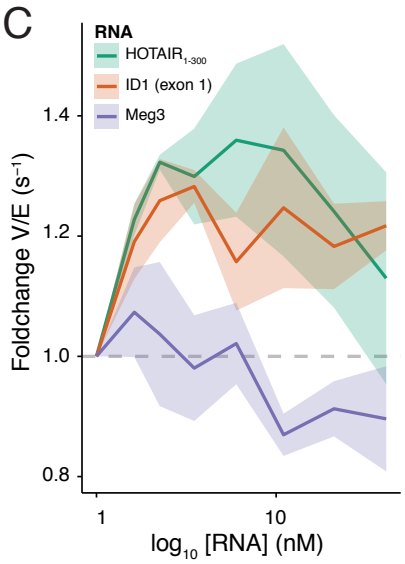

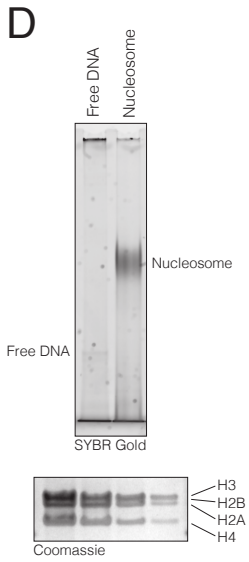

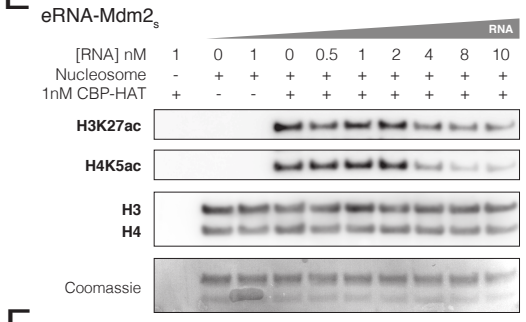

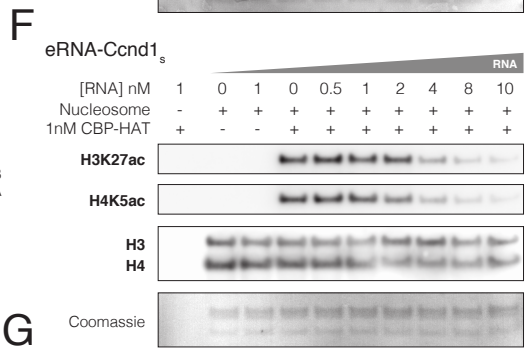

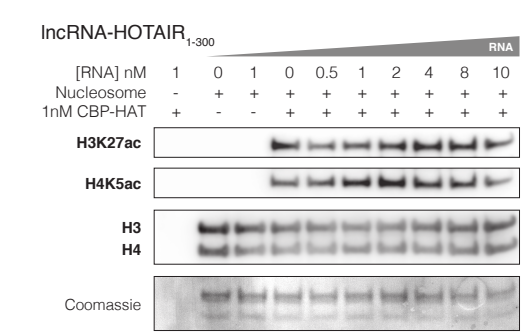

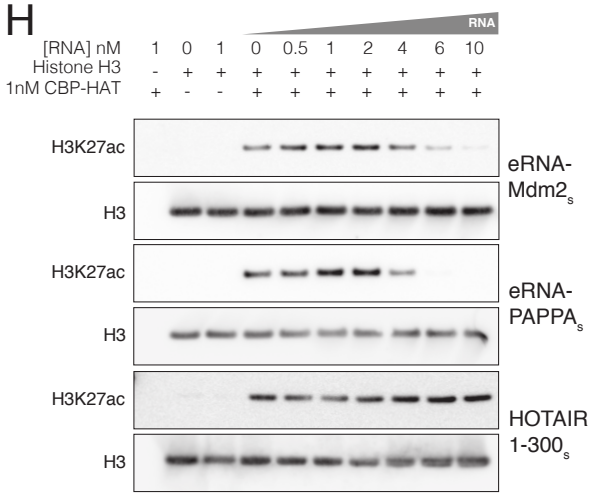

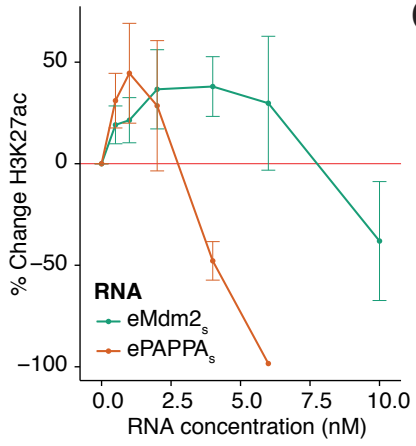

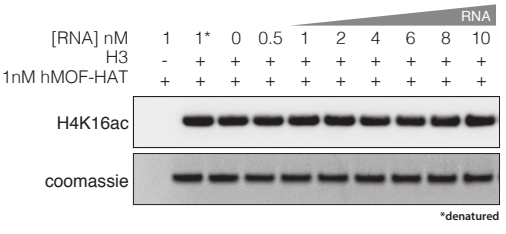

K

CBP-HAT	eRNA	$K_{m(H3-1-21)}$ (uM)	K_{cat} (s^{-1})	K_{cat}/K_m (M^{-1}/s^{-1})
wt	0nM RNA	44.55 +/- 3.99 (p=0.0001)	0.409 +/- 0.014 (p=7.97e^{-07})	9186.2 +/- 1102.3
wt	10nM RNA	26.42 +/- 3.55 (p=0.0007)	0.303 +/- 0.013 (p=2.86e^{-06})	11459.8 +/- 1948.2
mutant loop	0nM RNA	27.30 +/- 5.65 (p=0.0473)	0.714 +/- 0.048 (p=2.52e^{-05})	26139.5 +/- 7057.7
mutant loop	10nM RNA	27.96 +/- 8.97 (p=0.0263)	0.499 +/- 0.052 (p=2.18e^{-04})	17829.7 +/- 7488.5

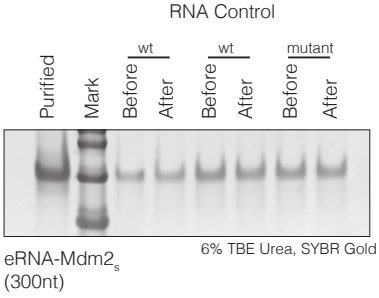

Supplemental Figure-6

Figure S6